2006

Microwave modeling and characterization of high-Tc superconducting thin films

Thamer Mousa Badarneh

United Arab Emirates University

Deanship of Graduate Studies

Microwave Modeling and Characterization of High-Tc Superconducting Thin Films

By

Thamer Mousa Badarneh

Supervised by

Dr. Maamar Benkraouda

Physics Department

Faculty of Science, UAEU

Dr. Mousa Issa Hussein

Electrical Engineering Department

Faculty of Engineering, UAEU

Dr. Hassan Ghamlouche

Physics Department

Faculty of Science, UAEU

A Thesis Submitted to the Deanship of Graduate Studies in Partial Fulfilment of the Requirements for Degree of Master of Science in Materials Science and Engineering

2005-2006

ES/F11

United Arab Emirates University
Graduate Studies
M.S.c. Program in Materials Science and Engineering

THESIS EXAMINATION REPORT

Student ID : 200350216
Student Name : Thamer Mousa Badarneh

Title of The Thesis : Microwave Modeling and Characterization of High-Tc Superconducting Thin Films.

The Thesis Examination as A Partial Fulfillment of M. Sc. Degree in Materilas Science and Engineering Was conducted on 8.4.2006. Based on Examining the Thesis and the Students Presentation and the Subsequent Discussion, The Committee Recommends:

☑ Thesis is Satisfactory as is.

☐ Thesis is Satisfactory After Minor Modifications.

☐ Thesis should be Re-Evaluated After Major Modifications.

☐ Thesis is Rejected.

Examining Committee Members:

Thesis Supervisor: Name: Maamar Benkraouda Signature: Date: 08/4/06

Co-advisor: Name: Mousa Hussein Signature: Date: 8/4/06

Co-advisor: Name: Hassan Ghamlouche Signature: Date: 08/04/06

Member : Name: Abdel Razik Sebak Signature: Date: 08/04/06

Member : Name: Dr. Hassan A.N. Hejase Signature: Date: 8/4/2006

Approval of Program Coordinator:

Dr. Yousef Haik ..... Date : 15/4/2006

APPROVAL:
Dean of Graduate Studies ..... Date : 26/4/06

Dedication

This thesis and all and all my future success are dedicated to very special people
To my beloved parents

Without their endless love, wisdom, guidance, support and enthusiasm
None of this could have been possible

Abstract

Because of the high critical temperature (Tc) that the new superconductors can reach, thin films can be used in a number of technological applications. One of the major applications of thin films is in the microwave devices, where superconducting strips are used as resonators, filters, delay lines, etc. The importance of the superconductors resides in the low losses incurred during the transmission along the strip. For example, the surface resistance of a high-Tc superconductor is at least one order of magnitude less than a similar one made of ordinary conductors. Because of this advantage, there is an increase in the use of superconducting strips instead of normal conductors in a number of electronic devices.

Modeling of different behaviors of the high-Tc superconductors are still phenomenological with a number of adjusting parameters, Because of the lack of knowledge about the real mechanisms behind the pairing occurring in the high-Tc superconductors. In a type-II superconductor, loss occurs mainly because of the motion of vortex, generated by either an external magnetic field or the self field of an applied current, due to the Lorentz force exerted by the current flowing in the superconductor. Therefore, the need to know the exact dynamics and hence the distribution of the current density in a superconductor is of primordial importance to calculate the loss incurred during Radio Frequency (RF) transmission. Because the nature of the pairing in the high-Tc superconductors is not settled yet, and the role of fluctuations due to high temperature, new phenomenological formula for different parameters, such as the penetration depth, the conductivity, etc, have to be taken into consideration, as well.

In this thesis, the FDTD method is formulated and applied to model the loss occurring during the transmission of an RF signal through superconducting microstrip. Different parameters including the surface impedance and current density distribution, as function of width and thickness, are calculated. The effect of temperature variation on these parameters is also investigated. It is found that they are temperature dependant.

Acknowledgments

First, always and foremost, I thank almighty Allah for his blessing and for providing me the capability to successfully complete this work.

I would like to express my heartiest thanks and sincere gratitude to my advisor, Dr. Maamar Benkraouda, for his guidance, support, encouragement, and patience. I wish also to express my sincere gratitude to Dr. Mousa Issa Hussein, for his unlimited assistance, critical reviewing and providing me the required facilities during the work. I wish to acknowledge my gratitude also to Dr. Hassan Ghamlouch, for his fruitful discussion, sincere guidance and being helpful during all phases of the work. I feel both honored and privileged to work with such a group.

I wish to express my sincere appreciation and great thanks to crown prince Faisal Ibn El-Hussein, who support me to take advantage of this opportunity.

I am deeply indebted to Maj. Abudullah Badarneh for his great help and support that makes this chance applicable. And I want to extend my thanks to Bgdr. Mohammed Ighrer and Col. Mahmod Almomani, for their helping and understanding of my situation.

Great thanks to Dr. Nihad Deeb from Jordan University of Science and Technology for his time and great help. Thanks to Mohammed Elsha`er, the lab technician in physics department labs, for helping in preparing some experiments.

Special appreciation is expressed to my colleagues and friends in UAE University, especially my dear friend Ahmed Embaby, for his great help especially in designing the presentation.

No words can ever express my great gratitude and special thanks to my great family, especially my parents for their great support and my wife for her great help throughout my study.

Table of Contents

List of Figures

Introduction

1.1 Introduction:

Superconductivity is perhaps one of the most fascinating phenomena that occur at low temperature. As opposed to conventional conductors, superconductors have the ability to conduct electrical current with very small resistance, no power loss, no generation of heat and greatly reduced levels of noise. The resistance is very small, but finite at microwave frequencies and zero at direct current (DC).

Until the last two decades, superconductivity phenomenon could be observed only at very low temperature attainable with expensive liquid helium. This phenomenon was explained by Bardeen, Cooper, and Schrieffer in what has become known as the BCS theory [1]. According to this theory, at a particular low temperature, called the transition temperature or critical temperature *(Tc)*, the electrons in certain materials pair up and form a single quantum state, acting like a frictionless fluid and becoming superconducting. However, High temperature superconductors (HTS) materials discovery in 1986, considered one of the great breakthroughs in the history of superconductivity. Before that time, the superconducting materials where known as Low-Temperature superconductor (LTS) materials. The new HTS materials have the capability to be superconducting at the boiling point of liquid nitrogen. Hence, scientists all over the world excited again to analyze, theorize and characterize the superconductivity phenomena, and explore their promising features and potential applications.

Basically, superconductivity is a multidisciplinary field. It spans almost the entire realm of physics and electrical engineering; including electronic, microwave, power, and computer engineering. In the last few years, there has been a growing interest in the application of high-temperature superconducting (HTS) materials. The application of this technology includes: electrical transmission cables, motors, generators, fault current limiters, superconductor magnetic energy storage systems (SMESs), magnetic resonance imaging (MRI), and high-speed computing. However, for the electromagnetism community, the application of HTS materials appears to be of great importance, for example, in the design of microwave circuits and antennas, and in the development of a variety of devices based on planar transmission lines.

1.2 Microwave properties of HTS:

The resistance of HTS does not drop to zero for alternating-current (AC) applications as in DC applications. The reason for the energy dissipation in AC applications is that; the high-frequency magnetic field penetrates a thin surface layer and induces oscillations of the electrons which are not bound in Cooper pairs. The power dissipation caused by the motion of the unpaired electrons can be characterized by a surface resistance [2]. This surface resistance of superconductor materials is still at least one order of magnitude smaller than that of conventional conductors at an operating temperature of 77k. The variation of surface resistance with frequency has been seen experimentally [3]. It varies with frequency as $(f)^2$, while it varies as $(f)^{1/2}$ for conventional conductors.

Another important characteristic that needs to be mentioned is the Meissner effect. It is the ability of the superconductor to expel the magnetic field. It is related to perfect diamagnetism but is actually a distinct effect, since the magnetic field will be zero inside the material in the superconducting state regardless of what it was before the material became superconducting. It determines the maximum (critical) magnetic field and current density before the superconducting material can be driven to the normal state. So, an attention should be made to the value of the applied field and the maximum current that can be carried by the superconductor. The Meissner effect is based on two principles - Lenz's Law and superconductivity. Due to Lenz's law the introduction of a magnetic field will cause "screening currents" at the surface of the superconductor that will expel the magnetic field. One of the theoretical explanations of the Meissner effect comes from the London equation. It shows that the magnetic field decays exponentially inside the superconductor over a distance described in terms of a parameter called the London penetration depth.

The frequency independent nature of the London penetration depth, which determines field penetration into the superconductor, is another property for the superconducting materials. This penetration depth with the surface resistance makes HTS very suitable for microwave application. They are used in a thin film form by being deposited in an

appropriate dielectric substrate. The current distribution inside the superconductor has to be calculated, in order to extract the surface resistance and penetration depth. This can be done by numerical simulation, and this is one of the objectives of this work. In general, microwave losses of HTS films depend on several factors such as the substrate material, deposition technique and to what extent the deposition conditions have been optimized [4].

Many theories have been developed to characterize the superconductivity phenomenon from a microscopic point of view: the BCS theory, the London Theory [5] and the Ginzburg–Landau (GL) theory [6]. The BCS theory gives an acceptable macroscopic explanation of why metals become superconducting at low temperatures. The other two theories have been used in integration with Maxwell's equations to model the microwave characteristics of superconducting devices. Based on the two-fluid model, the London theory explained successfully several characteristics of superconducting materials. But it does not take into consideration the field dependence of the constituent parameters of the superconducting material. On the other side, the Ginzburg–Landau (GL) theory is a more comprehensive macroscopic theory that accounts for field dependence, so the nonlinearities of the superconducting materials can be characterized [7].

Advantages of using HTS's at high frequency include: very small losses; which means low attenuation and low noise, very small dispersion up to frequencies of several tens of GHz, smaller devices due to lower losses, and the propagation time can be greatly reduced because of smaller size and the shorter interconnects [8]. As a result the implementation of high-Q resonators, long delay lines and low-loss filters with a sharp frequency response becomes possible [9].

1.3 HTS materials for microwave applications:

Practical realizations of microwave components using HTS technology have, for the most part, centered on the use of microstrip designs using thin-film technology. Among many HTS materials, both yttrium-based (YBCO) with Tc of 90K, and thallium-based

(TBCCO) with Tc over 100K, are considered the work horse for microwave application [7]. They have been used in thin-film form in the production of HTS microwave devices, which are essentially solid-state devices fabricated in a similar fashion as microprocessors and other semiconductor components.

Both YBCO and TBCCO can be formed into thin or thick films. Thick films are polycrystalline and are usually coated on a three-dimensional RF structure. Thin films are usually $\leq 1\mu m$ thick and are epitaxially grown on a substrate to form a single crystal; the resulting HTS wafer is then fabricated into planar RF structures. Thin-film deposition can be accomplished in a number of ways, but the most popular are pulsed laser deposition and co-evaporation, depending upon the material used [10].

Specialized materials such as LaAlO3, MgO and sapphire (Al2O3) are usually selected for the substrate. In addition to having good microwave properties, many other features should be taken into consideration for the selection of substrate, like: chemical compatibility between HTS films and substrate, substrate-film reactions, crystalline perfection, environmental stability, mechanical properties, thermal expansion and also cost [11].

1.4 Numerical methods for modeling Superconductivity:

Despite recent advances in the development of applied superconductivity, further improvements are necessary in view of the large-scale industrial applications of the current state-of-the-art superconducting materials. Modeling tools for superconductors are required since theoretical or analytical solutions of current distribution and field equations have been found for simple geometries only or even do not exist. Hence, numerical electromagnetic field analysis of HTS is a very useful tool so as the electromagnetic phenomena inside the superconductors can be visualized. A vast array of numerical methods is available for conventional conductors, and many of these are available in convenient Computer Aided Design (CAD) packages, where both two- and three- dimensional fields' solvers are available. With the increasing interest in superconductivity, a number of commercial CAD packages allow for complex impedance boundary conditions, thus allowing superconductors to be included in the

problem, although they do not necessarily solve problems when there is penetration into films. Conventional numerical techniques used in CAD and other numerical packages are able to cope with the problems of superconductivity by the introduction of complex conductivity [12].

A number of specific numerical techniques used with superconductors have been discussed in the literature. These include: mode matching technique is used to investigate a coplanar waveguide structure [13], the spectral domain volume integral equation (SDVIE) [14-15] method have been proposed to analyze superconducting microstrip lines, striplines and coplanar waveguides. Both the mode matching technique and the SDVIE method take into account the current distribution within the volume of the superconductor, giving results which show the effect of kinetic inductance and loss. However, these two methods are computationally inefficient and other related techniques are available in order to speed up computation. Another method is the efficient full-wave method using the equivalent surface impedance (ESI) approach [16]. The ESI is developed to calculate the effective dielectric constant, attenuation and characteristic impedance of superconducting microstrip lines and coupled lines on anisotropic substrate. The spectral domain immittance approach (SDIA) together with the complex boundary condition was proposed to analyze the microstrip structure with isotropic or anisotropic substrates [17-18]. However, this method is limited to the structures whose strip thickness, in comparison with the penetration depth, is very thin or very thick. A modified spectral domain approach is applied to study the propagation characteristics of high temperature superconducting microstrip lines whose signal strip and ground plane are of arbitrary thickness [9].

A numerical code based on the finite element (FE) method was tuned to perform electromagnetic field analysis of rectangular HTS with a large aspect ratio [19]. But it requires an optimization of mesh systems for accurate and efficient numerical analysis. However, the most notable in this respect is the finite difference time domain (FDTD) method [7], [20-22]. In [20] a 3D superconducting coplanar waveguide structure is simulated using the 3D FDTD method with a graded mesh. A full-wave FDTD is used to study the anisotropy associated with HTS planar structures and for modeling the nonlinearity in HTS microwave and millimeter-wave devices [7], [21]. Whereas in [22] an electromagnetic field simulator based on the FDTD method has been developed to

investigate a superconducting microstrip resonator. Although the FDTD method has many attractive features which will be discussed later, but one commonly known disadvantage of the FDTD is that it requires large amount of memory space and CPU time.

In this thesis, through providing a FDTD model for the microwave characteristics of HTS microstrip line, we attempt to be a part of the research going on this field.

Our developed code and associated numerical results may be used to design HTS microwave devices and circuits, the basics of FDTD technique and its capabilities are discussed in chapter II. In chapter III, we provide a theoretical analysis of the microwave properties of HTS, based on the two-fluid model and the London theory in conjunction with Maxwell's equation. The implementation of the HTS model through a FDTD code for a 3-D microstrip line is presented in chapter IV. The propagation characteristics, current density distribution and the surface impedance along with other parameters have been studied and analyzed. Simulations are carried out using a PC, not on a workstation or supercomputer. Finally conclusions and some of the proposed future works are listed in chapter V.

Finite Difference Time Domain Method (FDTD)

2.1 Introduction:

The finite difference time domain (FDTD) is a numerical technique for solving direct time Maxwell's equations. It was originated by Yee in 1966 [23]. It offers many advantages as an electromagnetic modeling, simulation and analysis tool. It is capabilities include [24]: arbitrary three-dimensional modeling, simulation of electromagnetic field interaction with objects of arbitrary conductivity and frequency dependant materials and predicting the response of system such as; scattered field, radiation pattern, radar cross-section, currents, penetration depth and interior coupling and scattering parameters for a given excitation. The main disadvantage of the method is its requirement of large computer memory and long computation time for three dimensional and large scale two dimensional problems. The overcoming of the difficulty depends on two aspects: the advancement of computers and improvement on the method it self [25].

FDTD is relatively simple in concept and execution. It is a marching-in-time procedure which simulates the actual continuous waves by sampled-data numerical analogs propagating in a computer data space. Where the basis of the FDTD code is the two Maxwell's equations in time-domain, these equations are expressed in a linearized form by means of central finite differencing, only nearest neighbor interactions need to be considered as the fields are advanced temporally in discrete time steps over spatial cells of rectangular shape [24].

2.2 FDTD Formulation:

2.2.1 Maxwell's equations:

The formulation of the FDTD method begins by considering the differential form of the Maxwell's two curl equations which govern the propagation of electromagnetic waves, where the differential time-domain Maxwell's equations in linear isotropic and frequency independent medium are given as [24]:

$$\nabla x\vec{E} = -\mu\frac{\partial\vec{H}}{\partial t} \qquad (2.1)$$

$$\nabla x\vec{H} = \varepsilon \frac{\partial \vec{E}}{\partial t} + \vec{J} \tag{2.2}$$

Where $\vec{E}$ is the electric field, $\vec{H}$ is the magnetic field, μ is the magnetic permeability, ε is the electric permittivity, and $\vec{J}$ is the conduction current density. Where $\vec{J} = \sigma\vec{E}$ is used to allow for lossy dielectric material, and σ is the electric conductivity.

These are all the information needed to completely specify the field behavior in linear isotropic materials as long as the initial distribution is specified and satisfied Maxwell's equations. The initial time is often taken to be zero, and the field quantities and resources are set to zero at that time.

Equations (2.1) and (2.2) can be rewritten into the form used for FDTD as:

$$\frac{\partial \vec{H}}{\partial t} = -\frac{1}{\mu} \nabla x\vec{E} \tag{2.3}$$

$$\frac{\partial \vec{E}}{\partial t} = \frac{1}{\varepsilon} \nabla x\vec{H} - \frac{\sigma}{\varepsilon} \vec{E} \tag{2.4}$$

Considering a rectangular coordinate system (x, y, z), then equations (2.3) and (2.4) can be rewritten in component form as:

$$\frac{\partial H_x}{\partial t} = \frac{1}{\mu}\left[\frac{\partial E_y}{\partial z} - \frac{\partial E_z}{\partial y}\right] \tag{2.5}$$

$$\frac{\partial H_y}{\partial t} = \frac{1}{\mu}\left[\frac{\partial E_z}{\partial x} - \frac{\partial E_x}{\partial z}\right] \tag{2.6}$$

$$\frac{\partial H_z}{\partial t} = \frac{1}{\mu}\left[\frac{\partial E_x}{\partial y} - \frac{\partial E_y}{\partial x}\right] \tag{2.7}$$

$$\frac{\partial E_x}{\partial t} = \frac{1}{\varepsilon}\left[\frac{\partial H_z}{\partial y} - \frac{\partial H_y}{\partial z} - \sigma E_x\right] \tag{2.8}$$

$$\frac{\partial E_y}{\partial t} = \frac{1}{\varepsilon}\left[\frac{\partial H_x}{\partial z} - \frac{\partial H_z}{\partial x} - \sigma E_y\right] \tag{2.9}$$

$$\frac{\partial E_z}{\partial t} = \frac{1}{\varepsilon}\left[\frac{\partial H_y}{\partial x} - \frac{\partial H_x}{\partial y} - \sigma E_z\right] \tag{2.10}$$

This system of six coupled partial differential equations (2.5-2.10) forms the basis of the FDTD algorithm for electromagnetic wave interactions with general three dimensional objects.

2.2.2 Yee algorithm:

Yee [23] introduced a set of finite-difference equations for the system of equations (2.5-2.10), following Yee notation, we denote a space point in a rectangular grid as:

$$(i, j, k) = (i\Delta x, j\Delta y, k\Delta z) \tag{2.11}$$

And any function of space and time in this rectangular grid at point (i, j, k) is given by:

$$F^n(i,j,k) = F(i\Delta x, j\Delta y, k\Delta z, n\Delta t) \tag{2.12}$$

Where Δx, Δy, and Δz are the grid space increment in the *x, y, and z* coordinate directions. Δt is the time increment, and *i, j, k, and n* are integers.

The Yee FDTD algorithm is applied on a staggered grid as shown in figure 2.1. The Cartesian components of the electric field are the unknowns on one grid and the Cartesian component of the magnetic field are the unknowns on the second grid offset from the first by a half-cell distance in each Cartesian direction. This is known as the centered difference with a second order accuracy [24]. The space derivatives can be expressed as:

$$\frac{\partial F^n(i,j,k)}{\partial x} = \frac{F^n(i+0.5,j,k) - F^n(i-0.5,j,k)}{\Delta x} + O(\Delta x^2) \tag{2.13}$$

Similarly the time derivative can be expressed in the same manner:

$$\frac{\partial F^n(i,j,k)}{\partial t} = \frac{F^{n+0.5}(i,j,k) - F^{n-0.5}(i,j,k)}{\Delta t} + O(\Delta t^2) \tag{2.14}$$

To achieve the accuracy of (2.14), the electric field and the magnetic field values on the two grids are evaluated at alternate half time steps (leap-frog manner).

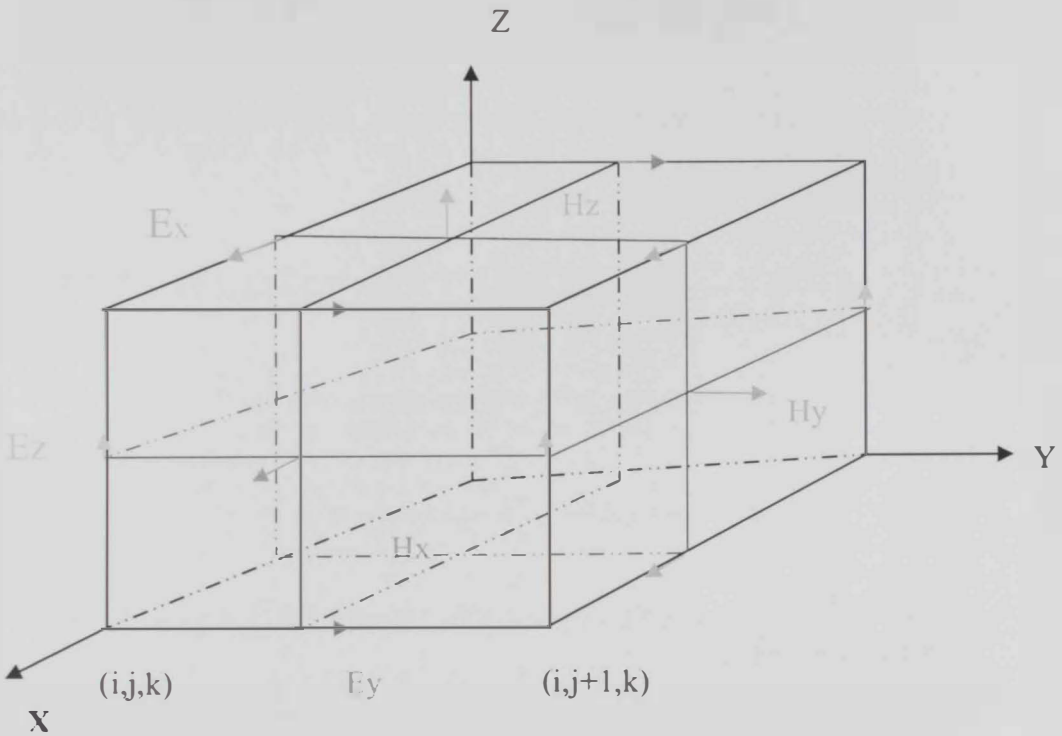

Figure 2.1: Yee cell geometry

Implementation of these expressions to (2.5-2.10) results in a system of six difference equations. The following are the six FDTD expressions for the magnetic and electric field components, respectively:

$$H_x^{n+0.5}(i, j+0. \quad \frac{\Delta t}{\mu(i, j+0.5, k+0.5)}$$

$$\left\{\left[E_y^n(i, j+0.5, k+1) - E_y^n(i, j+0.5, k)\right]/\Delta z\right.$$

$$\left.+\left[E_z^n(i, j, k+0.5) - E_z^n(i, j+1, k+0.5)\right]/\Delta y\right\} \qquad (2.15)$$

$$H_y^{n+0.5}(i+0.5, j, k+0.5) = H_y^{n-0.5}(i+0.5, j, k+0.5) + \frac{\Delta t}{\mu(i+0.5, j, k+0.5)}$$

$$\left\{\left[E_z^n(i+1, j, k+0.5) - E_z^n(i, j, k+0.5)\right]/\Delta x\right.$$

$$\left.+\left[E_x^n(i+0.5, j, k) - E_x^n(i+0.5, j, k+1)\right]/\Delta z\right\} \qquad (2.16)$$

$$H_z^{n+0.5}(i+0.5, j+0.5, k) = H_z^{n-0.} \quad \frac{\Delta t}{\mu(i+0.5, j+0.5, k)}$$

$$\left\{\left[E_x^n(i+0.5, j+1, k) - E_x^n(i+0.5, j, k)\right]/\Delta y\right.$$

$$\left.+\left[E_y^n(i, j+0.5, k) - E_y^n(i+1, j+0.\right.\right. \qquad (2.17)$$

$$E_x^{n+1}(i+0.5, j, k) = \frac{1-\dfrac{\sigma(i+0.5, j, k)\Delta t}{2\varepsilon(i+0.5, j,}}{1+\dfrac{\sigma(i+0.5, j, k)\Delta t}{2\varepsilon(i+0.5, j, k)}} E_x^n(i+0.5, j, k) + \frac{\Delta t}{\varepsilon(i+0.5, j, k)} \frac{1}{1+\dfrac{\sigma(i+0.5, j, k)\Delta t}{2\varepsilon(i+0.5, j, k)}}$$

$$\left\{\left[H_z^{n+0.}\right.\right.$$

$$\left.\left.+\left[H_y^{n+0.}\right.\right.\right. \qquad (2.18)$$

$$E_y^{n+1}(i,j+0.5,k)=\frac{1-\frac{\sigma(i,j+0.5,k)\Delta t}{2\varepsilon(i,j}}{1+\frac{\sigma(i,j+0.5,k)\Delta}{2\varepsilon(i,j+0.5,k)}}E_y^n(i,j+0.5,k)+\frac{\Delta t}{\varepsilon(i,j+0.5,k)}\frac{1}{2\varepsilon(i,j+0.5,k)}$$

$$\left\{\left[H_x^{n+0.}\right.\right.$$

$$\left.\left.+\left[H_z^{n+0.5}(i-0.5\quad H^{n+0.5}\quad\right]/\right\}\right. \tag{2.19}$$

$$E_z^{n+1}(i,j,k+0.5)=\frac{1-\frac{\sigma(i,j,k+0.5)\Delta t}{2\varepsilon(i,j,k+0.5)}}{1+\frac{\sigma(i,j,k+0.\ \Delta}{2\varepsilon(i,j,k+0.5)}}E^n(i,j,k+0.5)+\frac{1}{\varepsilon(i,j,\quad 1+\frac{\sigma(i,j,k+0.5)\Delta}{2\varepsilon(i,j,k+0.5)}}$$

$$\left\{\left[H_y^{n+0.}\right.\right.\qquad\qquad\Delta$$

$$\left.\left.+\left[H_x^{n+0.}(i,j-0.5,k+0.5)-H^{n+0.}\right]/\Delta y\right\}\right. \tag{2.20}$$

2.3 Cell size determination:

The choice of cell size is critical in applying FDTD. It must be small enough to permit accurate results at the highest frequency of interest, and yet be large enough to keep resources requirements manageable. The fundamental constraint is that the cell size must be much less than the smallest wavelength (λ) for which accurate results are desired (i.e. $\Delta \le \frac{\lambda}{20}$) where Δ is the cell size.

A word of caution here is that FDTD is a volumetric computational method, so that if some portion of the computational space is filled with penetrable material, we must use the wavelength in the material to determine the maximum cell size. For problems containing electrically dense materials, this results in cells in the material that are much smaller than if only free space and perfect conductors were being considered. The use of uniform cell size through out the hall problem space will be relatively small. This may greatly increase the number of cells needed. Possible measures to deal with this include the use of nonuniform cells (smaller cells in the dense material, larger cells outside) or graded mesh generator or surface or sheet "impedance" methods [26]. The total size of the FDTD space in cells is determined, after the cell size has been determined and the

number of cells needed to model the object and a reasonable amount of free space between the object and the outer boundary in each dimension is found.

2.4 Time step and stability:

When implementing any numerical method it is necessary to establish the conditions under which stability of the technique can be insured. For the FDTD method stability implies that as time marching continues, according to the Yee algorithm, the electric and magnetic field values must remain bounded.

As stated before, the FDTD method approximates Maxwell's equations as a set of finite difference equations. This approach is useful only when the solution of the difference equations is convergent and stable. Convergence means that, as the discrete step size approaches zero, the solution of the difference equation converges to the solution of Maxwell's equation. Thus, the problem of stability is a set of conditions, under which the error of the difference equation solution is finite. An investigation of the numerical stability of Yee's algorithm was initially presented in [27]. The stability analysis is based upon finding the Fourier numerical-wave modes in the grid for both the electric and magnetic field components, and requiring that each Fourier mode be stable for arbitrary angles of propagation through out the mesh.

Enforcing the stability in the three-dimensional FDTD algorithm imposes a constraint on the maximum size of the time step Δt, relative to the spatial-grid increments. This is given by the Courant condition:

$$\Delta t \leq \frac{1}{c\sqrt{\frac{1}{\Delta x^2}+\frac{1}{\Delta y^2}+\frac{1}{\Delta z^2}}} \tag{2.21}$$

where, $c = 1/\sqrt{\mu\varepsilon}$ is the speed of light in the homogeneous material being modeled. Once the cell size is determined, the maximum size of the time step Δt immediately follows the Courant stability condition [26]. To understand the basis of the Courant condition, consider a plane wave propagating through a FDTD grid. In one time step, any point on this wave must not pass through more than one cell, because during one time step FDTD can propagate the wave only from one cell to its nearest neighbors.

Experience has indicated that for actual computations, the Δt value given by the equality in equation (2.21) will provide accurate results, and in most situations more accurate results may not be obtained by using a smaller value of Δt. However, exceptions to this occur. One situation in which the time step must be reduced relative to equation (2.21) is when the conductivity of the material is much greater than zero, which is the case for superconductors. For conducting materials ($\sigma > 0$), stable calculations require time steps smaller than Courant limit. This is usually not a problem, because in most calculations the time step size is set by the speed of light in free space. As the velocity in the conducting material will be smaller than in free space, the time step in a FDTD calculation that includes both free space and conducting materials will be such that the Courant limit will be satisfied everywhere. However, the short wave length inside highly conducting materials may require much smaller FDTD cell than in surrounding free space regions [26].

2.5 Source consideration:

Source treatment depends on the type of the problem being simulated. However, the source is generally imposed by specified field components in the computational domain to be known functions of time and/ or space. Specifically, the vertical electric field between the ground plane and a microstrip line is specified as a function of time, e.g. Gaussian pulse, which is used in our study. A sample microstrip structure used in most of the computation models is shown in figure 2.2.

The Gaussian pulse has a smooth waveform in time, and its Fourier transform is also a Gaussian pulse centered at zero frequency. These characteristics make the Gaussian pulse a perfect choice for investigation the frequency-dependant characteristics of microstrip circuits [24]. Beside being simple to implement. An ideal Gaussian pulse (shown in figure 2.3) which propagates in the y-direction has the following expression:

$$E(t, y) = \exp\left[-\frac{[(t - t_0) - \frac{y - y_0}{c}]^2}{T^2}\right] \qquad (2.22)$$

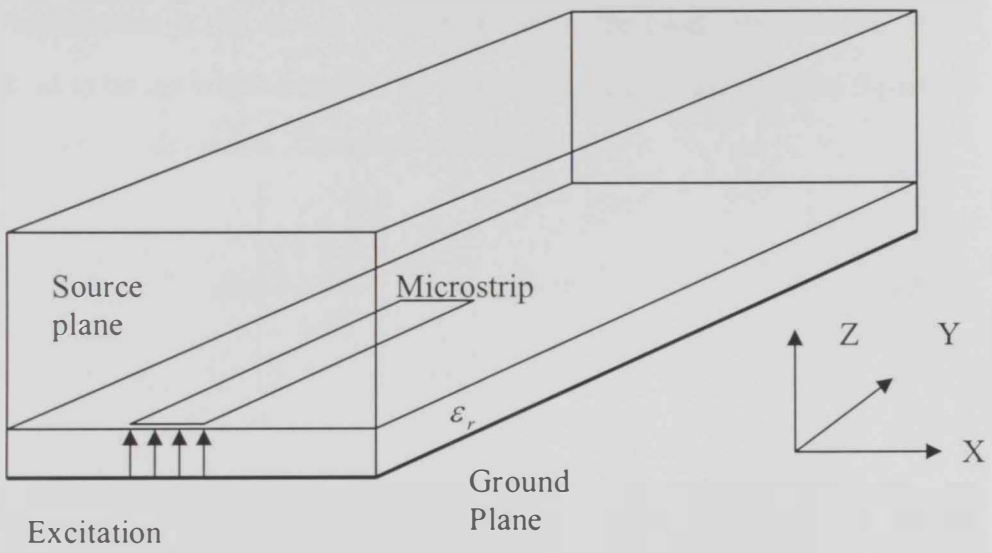

Figure 2.2: microstrip geometry and computational domain.

Where c is the velocity of the pulse in the specified medium, with the pulse being maximum for $y = y_0$ and $t = t_0$. The choice of the parameters T, t_0, and y_0 are subject to two requirements. First, the pulse must be wide enough to contain enough space divisions and at the same time to be narrow enough to maintain substantial amplitude within the frequency range of interest. For that, the space discretization interval Δy has to be small enough to model the smallest dimension of the structure and the time increment has to be small enough to meet the stability criterion discussed above. If this requirement is not met, a smaller Δy has to be used. The selected pulse width W is defined to be the width between the two symmetric points equal to 5 percent of the maximum value of the pulse. Therefore T is given by:

$$\exp\left[-\frac{\left(\frac{w}{2}\right)^2}{(cT)^2}\right] = \exp(-3)(\approx 5\%) \tag{2.23}$$

or

$$T = \frac{1}{\sqrt{3}} \cdot \frac{10\Delta y}{c} \tag{2.24}$$

By making this choice of T, the maximum frequency which can be calculated is:

$$f_{max} = \frac{1}{2T} = \frac{1}{2}\frac{\sqrt{3}c}{10\Delta y} \tag{2.25}$$

The second requirement is that the choice of y_0 and t_0 be made such that the initial turn on of the excitation will be small and smooth.

2.6 Absorbing Boundary Condition:

In general the electromagnetic analysis of scattering structures often requires the solution of "open region" problems, where the spatial domain of the computed fields is unbounded in one or more coordinate directions. Obviously, one cannot compute the solution over such a space, due to limitations in computer memory and computational time. As a result, it becomes necessary to truncate the computational domain in such a way as to make it appear infinite in extent by enclosing the structure by a suitable output

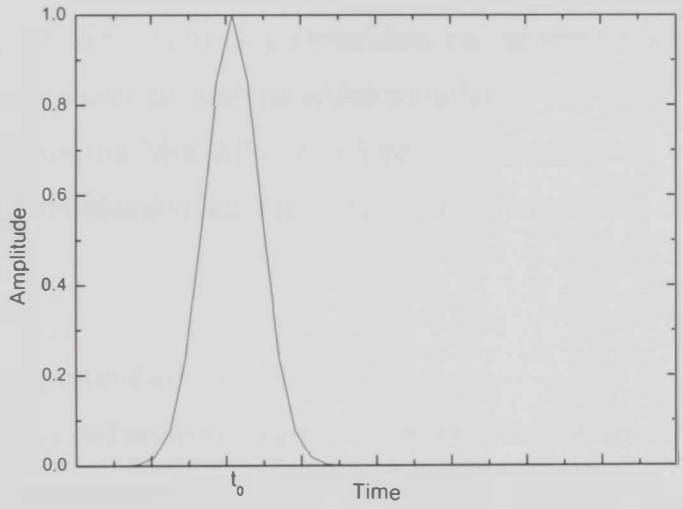

Figure 2.3: Ideal shape of Gaussian Pulse.

boundary that absorbs all outward traveling waves. Such a boundary is referred to as an absorbing boundary, or an absorbing boundary condition (ABC), and its function is to absorb all incident radiation and to suppress spurious back reflections of the outgoing wave.

The development of highly absorbing boundary conditions has been one of the most active areas in FDTD research. As stated above, the goal of an ABC is to absorb all outward traveling waves without producing any reflections. Although this goal is not entirely realistic since all ABCs produce some degree of back reflection, the better the ABC the lower the reflection will be. Some of the more common ABCs are Mur boundary conditions [28], super-absorbing boundary condition [29], and the perfectly matched layer (PML) method [30, 31]. Depending on the application, the level of back reflections that can be tolerated, and the added complexity one may choose to use either ABCs. In our work we use Mur ABC which provides a relatively reflection-free with easily implemented termination for the FDTD space. Mur ABC is discussed briefly below.

2.6.1 Mur absorbing boundary conditions:

The derivation of Mur radiation boundary condition is discussed in details in [24, 28]. The approximate representations of this condition have been found to be very effective when implemented using the differencing scheme proposed by Mur. As an application of such approximation to electromagnetic problems, we will take E_z at $x = 0$ for the three dimensional grid, which will be as follows;

First order Mur absorbing boundary condition:

$$E_z^{n+1}(0, j, k+0.5) = E_z^{n}(1, j, k+0.5) + \frac{c_0 \Delta t - \Delta x}{c_0 \Delta t + \Delta x}\left(E_z^{n+1}(1, j, k+0.5) - E_z^{n}(0, j, k+0.5)\right) \quad (2.26)$$

Second order Mur absorbing boundary condition:

$$
\begin{aligned}
E_z^{n+1}(0,j,k+0.5) &= E_z^{n-1}(1,j,k+0.5) \\
&+ \frac{c_0\Delta t-\Delta x}{c_0\Delta t+\Delta x}\left(E_z^{n+1}(1,j,k+0.5)-E_z^{n}(0,j,k+0.5)\right) \\
&+ \frac{2\Delta x}{c_0\Delta t+\Delta x}\left(E_z^{n}(0,j,k+0.5)-E_z^{n}(1,j,k+0.5)\right) \\
&+ \frac{\Delta x(c_0\Delta t)^2}{2(\Delta y)^2(c_0\Delta t+\Delta x)}\left(E_z^{n}(0,j,k+0.5)-2E_z^{n}(0,j,k+0.5)\right) \\
&+ \left(E_z^{n}(0,j-1,k+0.5)+E_z^{n}(1,j+1,k+0.5)\right. \\
&\left.- 2E_z^{n}(1,j,k+0.5)+E_z^{n}(1,j-1,k+0.5)\right) \\
&+ \frac{\Delta x(c_0\Delta t)^2}{2(\Delta z)^2(c_0\Delta t+\Delta x)}E_z^{n}(0,j,k+1.5)-2E_z^{n}(0,j,k+0.5) \\
&+ \left(E_z^{n}(0,j,k-0.5)+E_z^{n}(1,j+1,k+1.5)\right. \\
&\left.- 2E_z^{n}(1,j,k+0.5)+E_z^{n}(1,j,k-0.5)\right) \qquad (2.27)
\end{aligned}
$$

Due to the structure of the microstrip circuit, the pulses on the microstrip lines will be normally incident on the mesh walls. This leads to a simple approximation to the absorbing boundary conditions, which is the tangential fields on the outer boundary obey the one-dimensional wave equation in the direction normal to the mesh walls. This leads to a Mur first order absorbing boundary condition. It should be noted here that Mur second absorbing boundary conditions which account for oblique incident will not work on the mesh walls of the microstrip structure and yield an unstable solution [24].

High Temperature Superconductors (HTS) at Microwave Frequency

3.1 Introduction:

This chapter concentrates on the analysis of HTS at microwave frequencies based on the two-fluid model and the London theory in conjunction with Maxwell's equations. Extensive research has been carried out to study the high frequency effect in superconductors especially on LTS [32-36]. But the discovery of HTS [37] makes a great change in the view of microwave applications of superconductors, which led to an enormous expansion in theoretical and experimental research and application of HTS.

However, many theoretical and technological problems have to be solved before exploiting the HTS at microwave frequencies. Some of the technological problems are mentioned in chapter I, and are beyond the scope of this work. On the other hand, the theoretical level needs to define an appropriate physical and mathematical model suitable for integration of the electromagnetic theory and physical behavior of HTS. This provides an accurate representation of devices and circuits made of these materials. Another essential problem deals with the conduction mechanism inside the superconductor.

3.2 Theoretical analysis:

The theoretical analysis focuses on two main issues: the electromagnetic wave propagation during the transmission of an RF signal through a HTS microstrip line and the current distribution inside the HTS, and how their interaction influences the total system. So, a valid model for the microwave frequency band is needed to describe the current distribution as a function of the electric and magnetic fields. Since there is no accomplished theory of HTS superconductivity, phenomenological models are used. The phenomenological two-fluid model can predict macroscopically the relation between the local field and the current density. However, the complete solution is not achieved without taking into account the electromagnetic fields as a function of material specification, current densities, and boundary conditions. This can be achieved by properly introducing the HTS parameters through the constitutive relations of Maxwell's equations.

3.2.1 Two-Fluid model:

The two-fluid model describes the electrodynamics that results from the superposition of the response of the "superconducting" and "normal" electron fluids to alternating electromagnetic fields, where the total electron density n can be divided into two parts: the density of superconducting electrons ' n_s ' and that of normal electron ' n_n ' [38]. In other words, this model assumes that the conducting electrons in a superconductor are divided into two categories: superconducting electrons, known as Cooper pairs or electron pairs, and normal electrons.

In that manner, superconductivity in considered as a sequence of paired and unpaired electrons traveling within the lattice of a solid. The paired electrons travel, under the influence of an electric field, without loss. In addition, due to the thermal energy present in the solid, some of the electron pairs are split, so that some normal electrons are always present at temperatures above absolute zero. It is therefore possible to model the superconductor in terms of complex conductivity, depending on the two-fluid model [12]:

$$\sigma_{TF} = \sigma_1 - j\sigma_2 \tag{3.1}$$

The electron pair transport, is assumed to be collision-free, while the normal electron transport is governed by the momentum conservation equation as follows [8]:

$$m\frac{d\vec{v}_s}{dt} = -q\vec{E} \tag{3.2}$$

and

$$m\frac{d\vec{v}_n}{dt} + m\frac{\vec{v}_n}{\tau} = -q\vec{E} \tag{3.3}$$

where, $\vec{v}_s$ and $\vec{v}_n$ are the drift velocities of the charge carriers in the superconducting and normal states, respectively. q and m are charge and effective mass of the electron and τ is the relaxation time.

Therefore the total current density consists of two components; the superconducting current density $\vec{J}_s$ and the normal electron density $\vec{J}_n$:

$$\vec{J} = \vec{J}_s + \vec{J}_n = \sigma_{TF}\vec{E} \tag{3.4}$$

where

$$\vec{J}_s = qn_s\vec{v}_s \tag{3.5}$$

and

$$\vec{J}_n = qn_n\vec{v}_n = \sigma_n\vec{E} \tag{3.6}$$

where, σ_n is the normal conductivity of the superconductor and is assumed to be real. The simplest form of the superconducting and normal electron densities, which are related to the total electron density and temperature, are given by the following relations [39]:

$$n_s(T) = n_0\begin{cases}0, for T \geq T_c \\ 1-(T/T_c)^\gamma, for T \leq T_c\end{cases} \tag{3.7}$$

$$n_n(T) = n_0\begin{cases}1, for T \geq T_c \\ (T/T_c)^\gamma, for T \leq T_c\end{cases} \tag{3.8}$$

where T is the temperature, T_c is the critical temperature, n_0 is the total electron density in the superconductor, and γ is an exponent.

$n_s(T)$ is closely connected with the principle parameter of a superconductor $\lambda_L(T)$ – the penetration depth of a magnetic field, the so-called London penetration depth [30]

$$\frac{1}{\lambda_L^2(T)} = \frac{q^2 n_s(T)\mu_0}{m_s} \tag{3.9}$$

The London penetration depth can be measured experimentally. The measurement of $\lambda_L(T)$ is a way to find the experimental dependence of $n_s(T)$. The dependence is generally approximated by [30].

$$\lambda_L(T) = \frac{\lambda(0)}{\left[1-(\frac{T}{T_c})^\gamma\right]^{1/2}} \tag{3.10}$$

where, $\lambda(0)$ is the penetration depth for $T \to 0$. The relations (3.7)-(3.10) can be applied both to the low-temperature superconductors (LTS) with γ=4.0, and to HTS's with γ=1.3-2.1. This two-fluid model as applied to HTS's is called the enhanced or modified two-fluid model [39].

The above model paves the way to relate the superconducting and normal current densities to electromagnetic fields, enforcing the structure boundary conditions, we can solve for the associated electric and magnetic fields.

3.2.2 Superconductors and Maxwell's equations:

The equations governing the solution of the superconducting microstrip line problem are Maxwell's equations in addition to the constitutive relations for the current density combined from the two-fluid model and the London equation. The superconducting state fluid current density is obtained from London equation as follows:

$$\vec{J}_s = \frac{1}{i\omega\mu_0\lambda_L^2}\vec{E} \tag{3.11}$$

in the time domain, this equation becomes:

$$\frac{d\vec{J}_s}{dt} = \frac{1}{\mu_0\lambda_L^2}\vec{E} \tag{3.12}$$

The normal state current density is then obtained from ohm's law as in equation (3.6). It must be noted that these expressions are valid under the assumption of having an isotropic HTS material [21].

Maxwell's equations discussed in chapter II are modified for the superconductor case. The first equation becomes:

$$\nabla x\vec{H} = i\omega\varepsilon\vec{E} + \vec{J}_S + \vec{J}_n \tag{3.13}$$

Where $\vec{J}_S$ is the superconducting current density expressed in equation (3.11) and $\vec{J}_n = \sigma_n\vec{E}$ is the normal current density. And in the time domain, (3.13) reduces to:

$$\nabla x\vec{H} = \varepsilon\frac{d\vec{E}}{dt} + \frac{1}{\mu_0\lambda_L^2}\int\vec{E}dt + \sigma_n\vec{E} \tag{3.14}$$

and the second Maxwell's equation:

$$\nabla x\vec{E} = -i\omega\mu_0\vec{H} \tag{3.15}$$

becomes in the time domain:

$$\nabla x\vec{E} = -\mu_0\frac{d\vec{H}}{dt} \tag{3.16}$$

The combination of the two-fluid model, the London equation for the current density and Maxwell's equations provide a complete picture about the problem in hand, especially for the calculation of the surface impedance. An important point to mention here is that the amplitude of E and H, at any point and the total current density as well, are linearly dependant. This assumption should be taken into consideration in designing HTS transmission lines or devices.

FDTD and 3-D HTS microstrip

In chapter II, we have discussed the FDTD method concepts, and in chapter III we introduced theoretically the HTS model at microwave frequencies. The challenge now is to implement the HTS model through a FDTD code for the case of a 3-D superconducting microstrip to be used for designing microwave devices and circuits.

In this chapter the calculation of propagation characteristics, current density distributions and surface resistance are presented. These calculations assume that the wave propagation is quasi-TEM and that the magnetic field strength and current densities are low enough to insure that nonlinear effects may be ignored. The calculations of the above mentioned physical parameters of the HTS microstrip are very important not only for the designing of circuitry and devices, but also for characterizing the HTS materials themselves.

Experimentally, the microwave measurements [40-43] can determine the fundamental physical properties such as the penetration depth, critical temperature, and the real part of the conductivity, as well as the average critical current and magnetic field. However, an accurate calculation of the current distribution, resistance and electric and magnetic field distribution is an essential issue to accurately infer the fundamental physical properties.

4.1 FDTD and HTS:

The starting point of developing the simulation code is the modified Maxwell's equations for the superconducting case discussed in chapter III, where the implementation of these equations in a FDTD scheme will result in a system of six difference equations. However, it can be noticed that the magnetic field components remain the same as in equations (2.15-2.17), and the difference appears in the electric field components where the effect of the super current is included. So, the implementation of equation (3.13) in a FDTD expression for the electric field components for the superconducting case is given by:

$$E_x^{n+1}(i+0.5,j,k)=\frac{1-\frac{\sigma(i+0.5,j,k)\Delta t}{2\varepsilon(i+0.5,j,k)}}{1+\frac{\sigma(i+0.5,j,k)\Delta t}{2\varepsilon(i+0.5,j,k)}}E_x^n(i+0.5,j,k)-\frac{\Delta t}{\varepsilon(i+0.5,j,k)}\frac{1}{1+\frac{\sigma(i+0.5,j,k)\Delta t}{2\varepsilon(i+0.5,j,k)}}J_{sx}^{n+\frac{1}{2}}(i+0.5,j,k)$$

$$+\frac{\Delta t}{\varepsilon(i+0.5,j,k)}\frac{1}{1+\frac{\sigma(i+0.5,j,k)t}{2\varepsilon(i+0.5,j,k)}}\left\{\left[H_z^{n+\frac{1}{2}}(i+0.5,j+0.5,k)-H_z^{n+\frac{1}{2}}(i+0.5,j-0.5,k)\right]/\Delta y\right.$$

$$\left.+\left[H_y^{n+\frac{1}{2}}(i+0.5,j,k-0.5)-H_y^{n+\frac{1}{2}}(i+0.5,j,k+0.5)\right]/\Delta z\right\} \qquad (4.1)$$

$$E_y^{n+1}(i.j+0.5,k)=\frac{1-\frac{\sigma(i.j+0.5,k)\Delta t}{2\varepsilon(i.j+0.5,k)}}{1+\frac{\sigma(i.j+0.5,k)\Delta t}{2\varepsilon(i.j+0.5,k)}}E_y^n(i.j+0.5,k)-\frac{\Delta t}{\varepsilon}\frac{1}{1+\frac{\sigma\Delta t}{2\varepsilon}}J_{sy}^{n+\frac{1}{2}}(i.j+0.5,k)$$

$$+\frac{\Delta t}{\varepsilon}\frac{1}{1+\frac{\sigma(i.j+0.5,k)\Delta t}{2\varepsilon(i.j+0.5,k)}}\left\{\left[H_x^{n+\frac{1}{2}}(i.j+0.5,k+0.5)-H_x^{n+\frac{1}{2}}(i.j+0.5,k+0.5)\right]/\Delta z\right.$$

$$\left.+\left[H_z^{n+\frac{1}{2}}(i-0.5,j+1,k)-H_z^{n+\frac{1}{2}}(i+0.5,j+0.5,k)\right]/\Delta x\right\} \qquad (4.2)$$

$$E_z^{n+1}(i.j,k+0.5)=\frac{1-\frac{\sigma(i,j,k+0.5)\Delta t}{2\varepsilon(i,j,k+0.5)}}{1+\frac{\sigma(i,j,k+0.5)\Delta t}{2\varepsilon(i,j,k+0.5)}}E_z^n(i,j,k+0.5)-\frac{\Delta t}{\varepsilon(i.j.k+0.5)}\frac{1}{1+\frac{\sigma(i,j,k+0.5)\Delta t}{2\varepsilon(i,j,k+0.5)}}J_{sz}^{n+\frac{1}{2}}(i,j,k+0.5)$$

$$+\frac{\Delta t}{\varepsilon(i,j,k+0.5)}\frac{1}{1+\frac{\sigma(i,j,k+0.5)\Delta t}{2\varepsilon(i,j,k+0.5)}}\left\{\left[H_y^{n+\frac{1}{2}}(i+0.5,j,k+0.5)-H_y^{n+\frac{1}{2}}(i-0.5,j+0.5,k+0.5)\right]/\Delta x\right.$$

$$\left.+\left[H_x^{n+\frac{1}{2}}(i,j-0.5,k+0.5)-H_x^{n+\frac{1}{2}}(i,j+0.5,k+0.5)\right]/\Delta y\right\} \qquad (4.3)$$

Where J_{sx}, J_{sy} and J_{sz} are the superconducting current density components in the *(x,y,z)* directions, respectively. The value of these components can be obtained from the London equation, which in turn can be implemented in a FDTD scheme as follows:

$$J_{sx}^{n+\frac{1}{2}}(i,j,k) = J_{sx}^{n-\frac{1}{2}}(i,j,k) + \frac{\Delta t}{\mu_0 \lambda_L^2} E_x^n(i,j,k) \tag{4.4}$$

$$J_{sy}^{n+\frac{1}{2}}(i,j,k) = J_{sy}^{n-\frac{1}{2}}(i,j,k) + \frac{\Delta t}{\mu_0 \lambda_L^2} E_y^n(i,j,k) \tag{4.5}$$

$$J_{sz}^{n+\frac{1}{2}}(i,j,k) = J_{sz}^{n-\frac{1}{2}}(i,j,k) + \frac{\Delta t}{\mu_0 \lambda_L^2} E_z^n(i,j,k) \tag{4.6}$$

4.2 Problem Formulation:

The application of the FDTD approach to HTS structure at higher frequencies is clear now. However, some interesting features need to be discussed before formulating the final code for the problem at hand, so that the model can be robust and accurate. These features are necessary in order to successfully model the HTS microstrip line and devices, where field penetration effects needs to be taken into consideration. These features include: time step and cell size determination which led to a nonuniform graded mesh, the absorbing boundary conditions, and the improvement of the stability of the overall FDTD algorithm. Moreover, these features will help in using the FDTD method without resorting to a supercomputer.

Time step and cell size determination is one of the main issues in modeling HTS. The finite thickness of the HTS microstrip line, which is comparable to the penetration depth of the magnetic field inside the HTS, needs to be taken into consideration. For this reason, small mesh size is chosen inside and around the HTS microstrip line. In order to accurately model the effect of the penetration of the magnetic field into the HTS, the mesh size should be equal to a fraction of the penetration depth. Hence a dense mesh is needed to accurately model this finite thickness without any approximation, which requires non realistic memory storage. Recall that one of the main well known disadvantages of FDTD method is that it requires huge amount of memory space and CPU time.

Moreover, even for very small dimensions for the microstrip line. Absorbing Boundary Conditions must be placed at far enough from the line to avoid reflections which can affect the accuracy of the results, and enlarge the computational domain of the problem.

Hence it requires discretization of a large cross section of the line, which may be impossible to solve with most workstations.

To overcome such a problem, we need to minimize the mesh cells, in order to reduce the memory storage, and make the FDTD simulation robust and efficient, but in a way that will not affect the results. Many techniques found in literature such as: the variable mesh technique [20], non-uniform lattice [22], or graded nonuniform mesh generator [7, 21] are used to deal with this problem. All these techniques share the same principle where a small mesh around and within HTS is applied and larger meshes in the rest of the computational domain. However, the graded mesh technique is simpler than the other techniques, since no different smaller time step is required to update the electric and magnetic fields inside the smaller mesh cells.

For the graded mesh generator, the computational domain is discretized according to the following expression [19]:

$$\Delta x(i)_{i=1}^{i=n} = W * \left[\left(\frac{i}{n} \right)^{p} - \left(\frac{i-1}{n} \right)^{p} \right] \tag{4.7}$$

Where Δx is the mesh size, W is the distance to be discretized, n is the number of points, and p is the mesh resolution factor which must be minimized to reduce the dispersion introduced by the nonuniform descritization. This discretization is applied when it is necessary to use small meshes around and inside the HTS, however the rest of the computational domain may remain uniform, as can be seen in figure 4.1.

Because of these restrictions on the mesh cells, where it should be a fraction of the penetration depth, and the high conductivity of HTS, it results in very small time step. Following the Courant stability factor, the time step is chosen based on the smallest mesh size to satisfy these restrictions.

The computational domain should be closed by an absorbing boundary condition, which is discussed in chapter II, to overcome the problem in computer memory limitations and computational time. In our work we use Mur ABC which is a relatively reflection-free and is an easily implemented termination for the FDTD space.

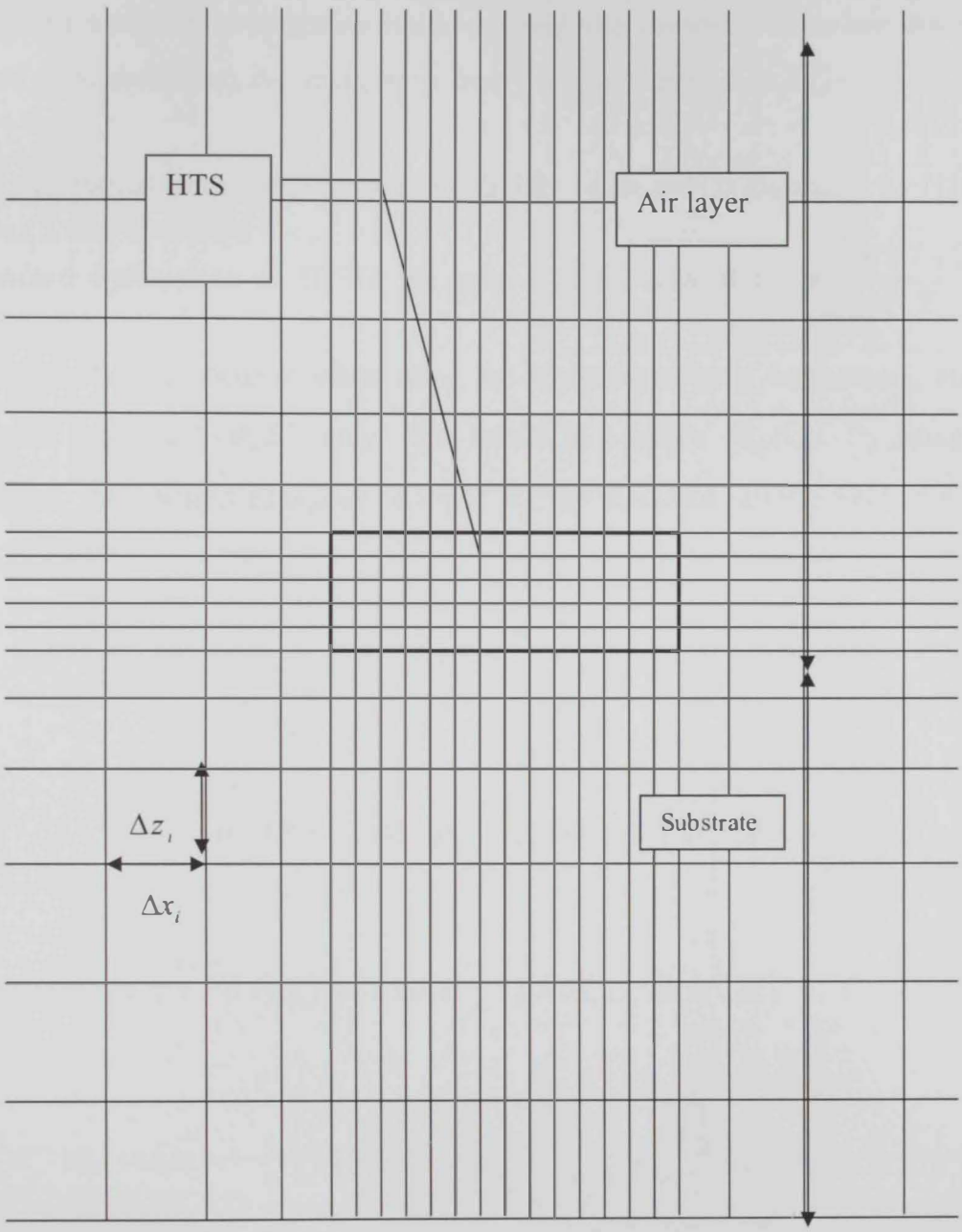

Figure 4.1: Graded Mesh Generator.

One final note is that special care should be taken when applying the absorbing boundary at the source plane. During the launching period of the Gaussian pulse no absorbing boundary is assigned to the plane, however, once the pulse has passed the source plane and starts propagating inside the grid, the absorbing boundary should be switched on to absorb any incoming wave from the computational grid [24].

A final step should be done to improve the stability of the FDTD algorithm for HTS. In the standard formulation of FDTD, the term $\sigma_n E$ is replaced by $\sigma_n\left(\frac{E^{n+1}+E^n}{2}\right)$.

Unstable results are obtained when using the above mentioned formulation. Hence, $\sigma_n E$ were replaced by $\sigma_n E^{n+1}$ only. This results in a stable solution. By using this formulation, the updated equations (4.1-4.3) for the modified electric fields for HTS will be as follows:

$$E_x^{n+1}(i+0.5,j,k)=\frac{1}{1+\frac{\sigma_n\Delta t}{2\varepsilon}}E_x^n(i+0.5,j,k)-\frac{\Delta t}{\varepsilon}\frac{1}{1+\frac{\sigma_n\Delta t}{\varepsilon}}J_{sx}^{n+\frac{1}{2}}(i+0.5,j,k)+\frac{\Delta t}{\varepsilon}\frac{1}{1+\frac{\sigma_n\Delta t}{\varepsilon}}$$

$$\left\{\left[H_z^{n+\frac{1}{2}}(i+0.5,j+0.5,k)-H_z^{n+\frac{1}{2}}(i+0.5,j-0.5,k)\right]/\Delta y\right.$$

$$\left.+\left[H_y^{n+\frac{1}{2}}(i+0.5,j,k-0.5)-H_y^{n+\frac{1}{2}}(i+0.5,j,k+0.5)\right]/\Delta z\right\} \qquad (4.8)$$

$$E_y^{n+1}(i,j+0.\qquad\frac{1}{1+\frac{\sigma_n\Delta t}{2\varepsilon}}E_y^n(i,j+0.5,k)-\frac{\Delta t}{\varepsilon}\frac{1}{1+\frac{\sigma_n\Delta t}{\varepsilon}}J_{sy}^{n+\frac{1}{2}}(i,j+0.5,k)+\frac{\Delta t}{\varepsilon}\frac{1}{1+\frac{\sigma_n\Delta t}{\varepsilon}}$$

$$\left\{\left[H_x^{n+\frac{1}{2}}(i,j+0.5,k+0.5)-H_x^{n+\frac{1}{2}}(i,j+0.5,k-0.5)\right]/\Delta z\right.$$

$$\left.+\left[H_z^{n+\frac{1}{2}}(i-0.5,j+0.5,k)-H_z^{n+0.5}(i+0.5,j+0.5,k)\right]/\Delta x\right\} \qquad (4.9)$$

$$E_z^{n+1}(i,j,k+0.5) = \frac{1}{1+\frac{\sigma_n \Delta t}{\varepsilon}} E_z^n(i,j,k+0.5) - \frac{\Delta t}{\varepsilon}\frac{1}{1+\frac{\sigma_n \Delta t}{\varepsilon}} J_{sz}^{n+\frac{1}{2}}(i,j,k+0.5) + \frac{\Delta t}{\varepsilon}\frac{1}{1+\frac{\sigma_n \Delta t}{\varepsilon}}$$

$$\left\{\left[H_y^{n+\frac{1}{2}}(i+0.5,j,k+0.5) - H_y^{n+0.5}(i-0.5,j,k+0.5)\right]/\Delta x\right.$$

$$\left.+\left[H_x^{n+\frac{1}{2}}(i,j-0.5,k+0.5) - H_x^{n+\frac{1}{2}}(i,j+0.5,k+o.5)\right]/\Delta y\right\} \qquad (4.10)$$

This step with the graded mesh makes it possible to calculate the characteristics of the HTS microstrip line and to improve the stability of the algorithm.

The electric field, the magnetic field and the superconducting current can be calculated and updated by the equations (2.15-2.20), equation (4.8-4.9) and equations (4.4-4.6). However in the case of normal conductor or dielectric only equations (2.15-2.20) are applied, and for the superconducting case equations (2.15-2.17), equations (4.8-4.9), and equations (4.4-4.6) are applied. So the propagation of an electromagnetic wave in the superconductor can be simulated.

4.3 Geometry and computational domain:

Figure 4.2 shows the construction of the superconducting microstrip line, the simulation target and the computational domain of the problem. The (YBCO) HTS microstrip line has a 50 Ω impedance with a strip width of 7.5 μm, and a thickness of 1 μm. Penetration depth and normal conductivity equal to 0.2 μm and $1.0X10^6 S/m$, respectively, at 77 K. the substrate thickness is 10 μm with $\varepsilon_r = 13$ which are used in [19]. A graded nonuniform mesh generator is used to discretize the computational domain as shown in figure 4.1, where the smallest mesh size is chosen inside and around the HTS microstrip line. The dimension of the computational domain is (64x100x30). The time step size is chosen based on the smallest mesh step size following the Courant stability condition. For simplicity, the ground plane is chosen to be a perfect conductor. The computational domain is terminated by Mur absorbing boundary conditions.

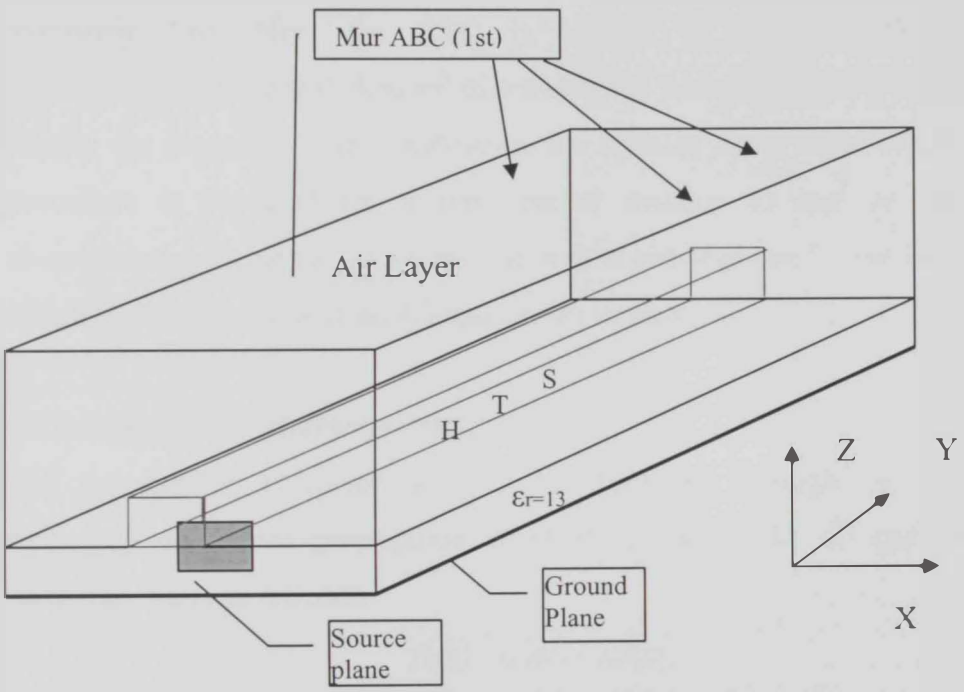

Figure 4.2 geometry and computational domain

4.4 Numerical results and discussion:

At time (t = 0) all field quantities are assumed to be zero throughout computational domain. At time ($\Delta t = 1$) an excitation pulse is launched underneath the HTS microstrip line at a distance equal ($10\Delta y$). The excitation pulse used is a Gaussian pulse which is discussed in chapter II; this pulse is assumed to have only the E_z component of the electric field. Then the electric field components are updated using equations (2.18-2.20) for the dielectric and air layer. Also equations (4.8-4.10) are used for HTS microstrip line. Next the ABC is applied to minimize the reflection. The superconducting current density distribution is calculated using equations (4.4-4.6). Finally the magnetic field components are updated using equations (2.15-2.17). This procedure is repeated for a time period suitable to analyze wave propagation characteristics inside the structure. The results obtained are for the HTS microstrip line which is described in section 4.3 and shown in figure 4.2.

4.4.1 Propagation characteristics:

The propagation characteristics can be discussed through the evaluation of the frequency dependant propagation constant γ. It can be divided into its real and imaginary parts as follows:

$$\gamma(\omega) = \alpha(\omega) + j\beta(\omega) \tag{4.11}$$

Where the real part, $\alpha(\omega)$, is commonly known as the attenuation constant, and the imaginary part, $\beta(\omega)$, as the phase constant. The attenuation constant is affected by the dielectric constant of the substrate as well as the conductor itself, whereas, the phase constant is mainly influenced by the geometry of the line.

For calculation of the two parts of the propagation characteristics $\alpha(\omega)$ and $\beta(\omega)$, we take the Fourier transform of $E_z(t)$ at two different positions underneath the center of the HTS microstrip, with separation ($L = L_2 - L_1$) along the propagation direction [24]:

$$E_z(\omega, y = L_1) = \int_{-\infty}^{\infty} E_z(t, y = L_1) e^{-j\omega t} dt \tag{4.12}$$

$$E_z(\omega, y = L_2) = \int_{-\infty}^{\infty} E_z(t, y = L_2) e^{-j\omega t} dt \tag{4.13}$$

Taking the ratio of (4.12) and (4.13), then the transfer function of this section of the HTS microstrip line will be as follows:

$$e^{-\gamma(\omega)(L_2-L_1)} = \frac{E_z(\omega, y = L_2)}{E_z(\omega, y = L_1)} \tag{4.14}$$

Where $\gamma(\omega)$ is as defined in (4.11).

To account for the dispersive characteristics of the HTS microstrip line, we need to calculate the effective dielectric constant $\varepsilon_{eff}(\omega)$. This can be defined from the phase factor $\beta(\omega)$ derived above, as follows:

$$\varepsilon_{eff}(\omega) = \frac{\beta^2(\omega)}{\omega^2 \varepsilon_0 \mu_0} \tag{4.15}$$

Figure 4.3 shows the temporal electric field propagation along the HTS microstrip line at two different positions. Small attenuation of the wave amplitude can be noticed along the propagation direction. The attenuation constant for the HTS microstrip is presented in figure 4.4. This shows a good agreement with results presented in [21]. For conventional conductors, copper for example, it has an attenuation constant on the order of (0.2 dB/cm) at 10 GHz and at operating temperature 77 K. In comparison, HTS microstrip has an attenuation constant about two order of magnitude less, on the order of (0.0025 dB/cm), which can be seen clearly from figure 4.4, provided that the surface resistance of the HTS microstrip is accurately modeled by the BCS theory. This proves the advantages of using HTS on microwave application over conventional conductors. Figure 4.5 shows the effective dielectric constant for HTS as function of frequency, which is comparable with the value calculated from the microstrip theory.

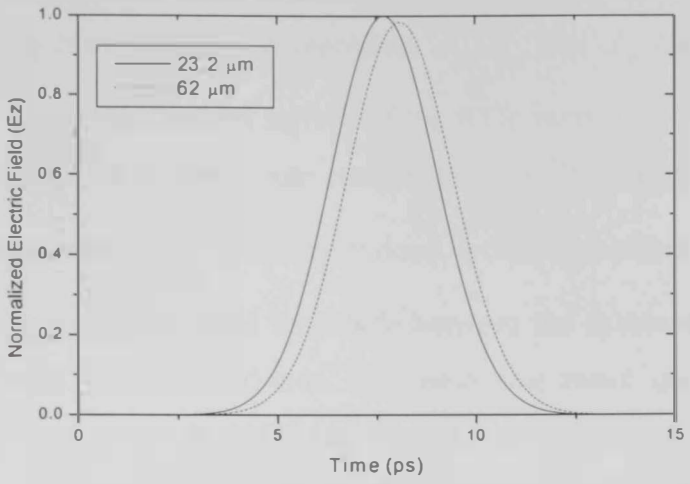

Figure 4.3: Normalized electric field under the HTS microstrip line at two different positions.

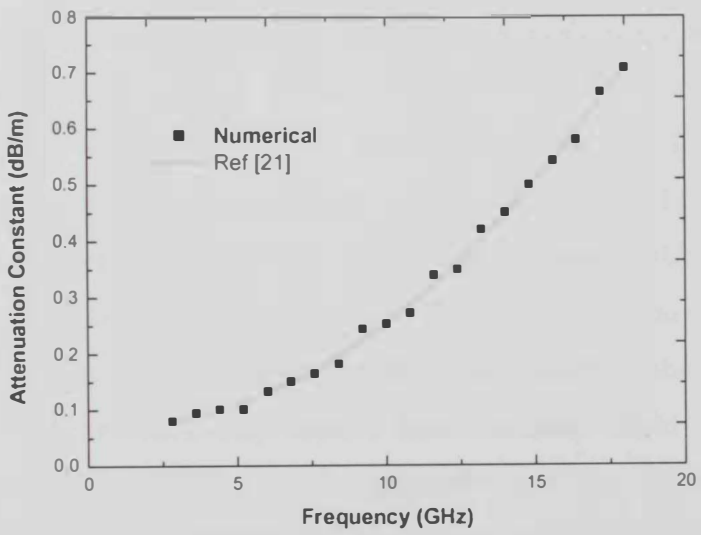

Figure 4.4: Attenuation constant for the HTS microstrip.

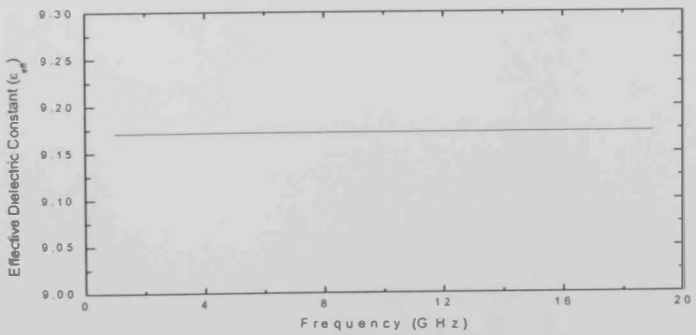

Figure 4.5: Effective dielectric constant for the HTS.

4.4.2: Current density distribution as function of width:

The superconducting current density components J_{sx},J_{sy} and J_{sz} are shown in figure 4.6 as function of time at the bottom surface of the HTS microstrip (it should be noted that they are normalized to the maximum component J_{sy}). The longitudinal component J_{sy} is the maximum component. This longitudinal current component is produced due to the variation in the magnetic field amplitude between the substrate and the HTS as can be seen in figure 4.7. This variation is a reasonable result due to the effect of magnetic field penetration into the HTS, and the difference in conductivity between the substrate and HTS. This agrees with ampere's law, which stated that, the line integral of the magnetic field over closed path is equal to the current enclosed.

The distribution of normalized longitudinal current density component (J_y), as function of the width at the bottom surface of the HTS microstrip, is shown in figure 4.8, for the total, normal and superconducting current densities. The superconducting current density is larger than the normal current density as expected. Because, the super electrons density that carries the super current is larger than that of the normal electrons carrying the normal current. The distribution of the current density becomes more uniform and almost constant as we go inside the HTS width as can be seen in figure 4.9, which shows the current density distribution along the width of the HTS microstrip. However, the current increases very rapidly near the strip edges due to the field singularity and the penetration effect of the magnetic field into the HTS. Figure 4.10 shows the distribution of the magnetic field around and within the HTS microstrip line width, which clearly shows the concentration of the maximum value of the magnetic field near the edges of the strip.

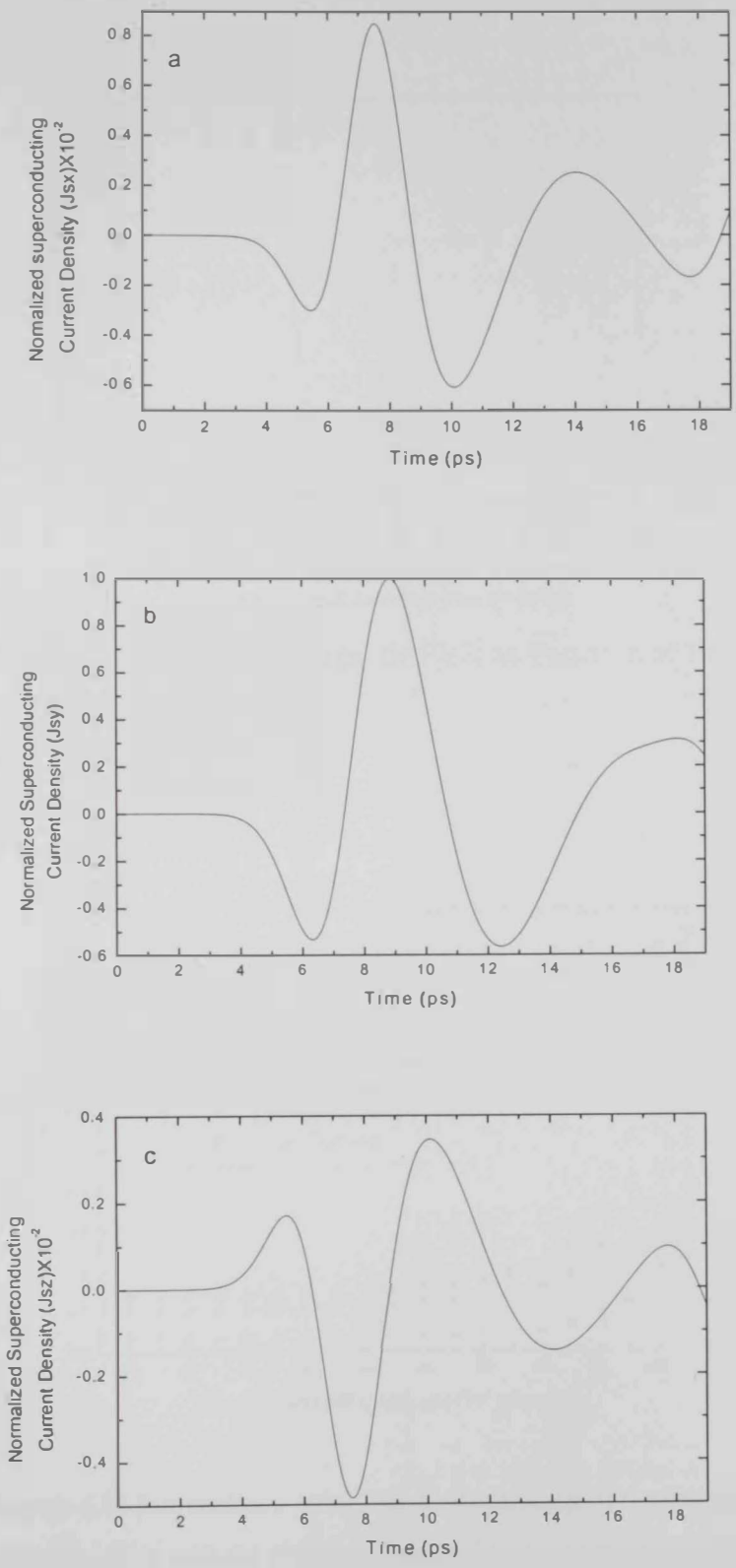

Figure 4.6: Normalized Superconducting Current Density. (a) Jsx, (b) Jsy, (c)Jsz. At the center of the width of bottom surface of HTS microstrip, and y =20Δy.

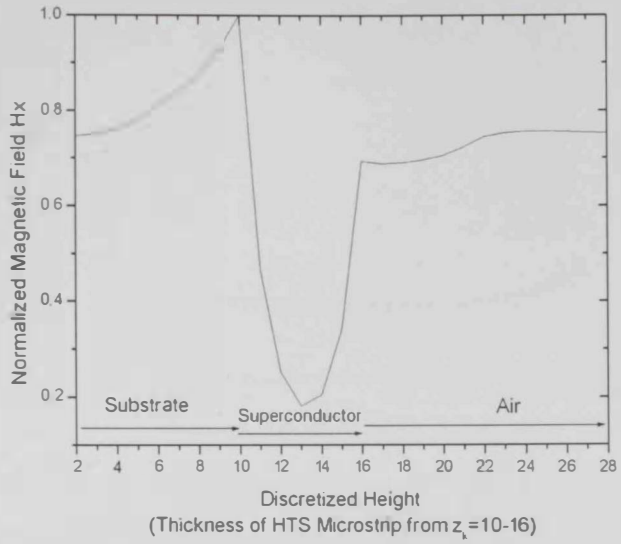

Figure 4.7: Normalized Magnetic Field as Function of Height.

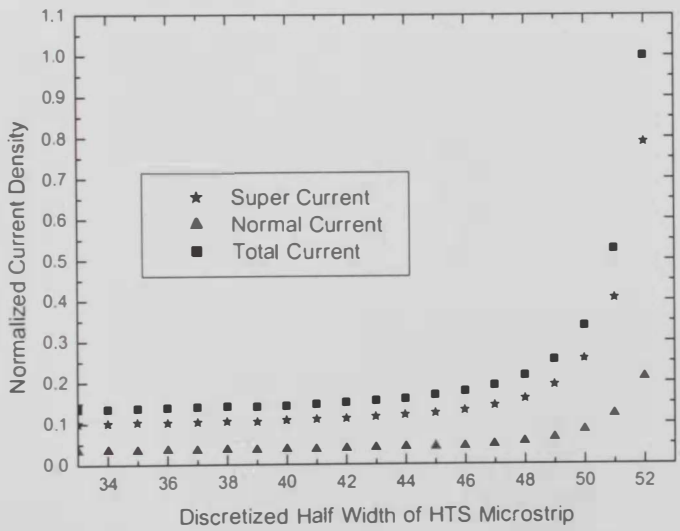

Figure 4.8: Normalized total, superconducting and normal current density at the bottom surface of the HTS microstrip and y= 20Δy.

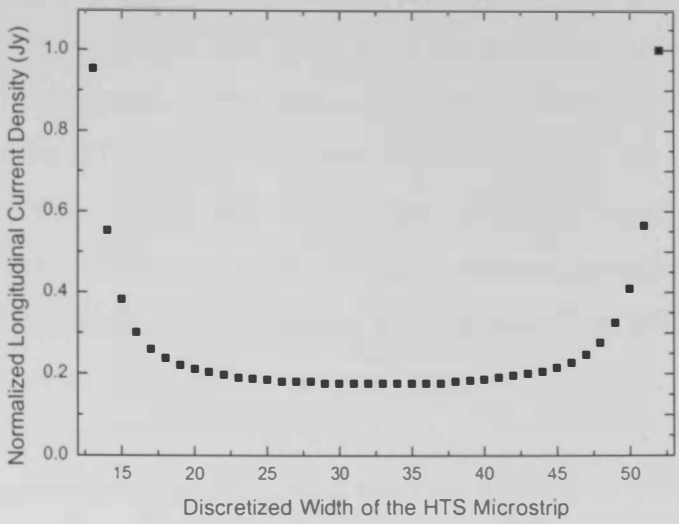

Figure 4.9: Normalized Current distribution as function of the width at the bottom surface of the HTS microstrip and y= 20Δy.

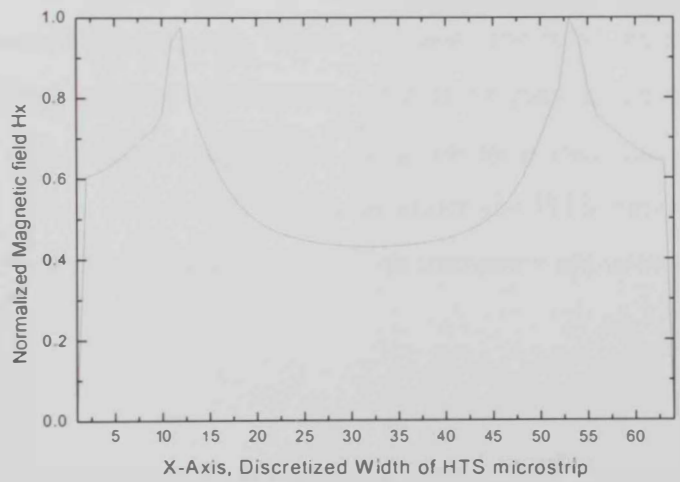

Figure 4.10: Normalized magnetic field distribution as function of the width. (HTS width form x_t=13-52).

4.4.3: Current density as function of thickness:

Another study was to investigate the behavior of the superconducting current with the thickness of HTS microstrip. The superconducting current density distribution at different values of the HTS thickness is shown in Figure 4.11. The maximum value of the current is in the surface adjacent to the substrate, which means that the superconducting surface adjacent to the substrate carries the main current. In other words, the current decreases as we go along the thickness of the HTS from the surface adjacent to the substrate, and slightly increases when we approach the total thickness (top surface of the HTS microstrip) which is shown schematically in figure 4.12. Figure 4.13 shows a clear view of the supercurrent density distribution as a function of width and height at the bottom of the HTS microstrip. This phenomenon is due to the dielectric constant material used as substrate [44]. This led us to investigate the dielectric constant and the superconducting current density distribution. Figure 4.14 shows the superconducting current density distribution as a function of HTS width at different dielectric constant. This proves that the current increases as the dielectric constant increases. However, the use of high dielectric constant accumulates the current on one side of the microstrip. But we should not forget the effect of the dielectric substrate under the HTS microstrip, which increases the field intensity at the bottom side. This effect may produce nonlinearity effects or may make the superconductor material lose its superconductivity if the field intensity increases over the limit of superconductivity. Thus, a dielectric substrate under the HTS material with relatively low dielectric constant may be favorable for high frequency applications.

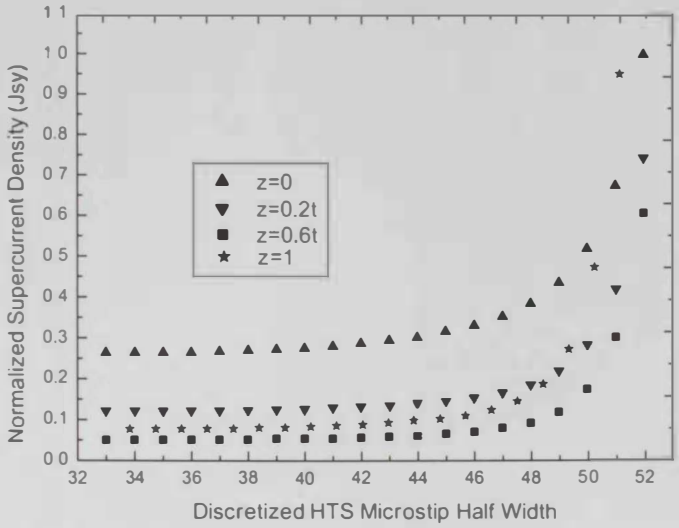

Figure 4.11: Superconducting Current Density Distribution as a function of width at different values of thickness.

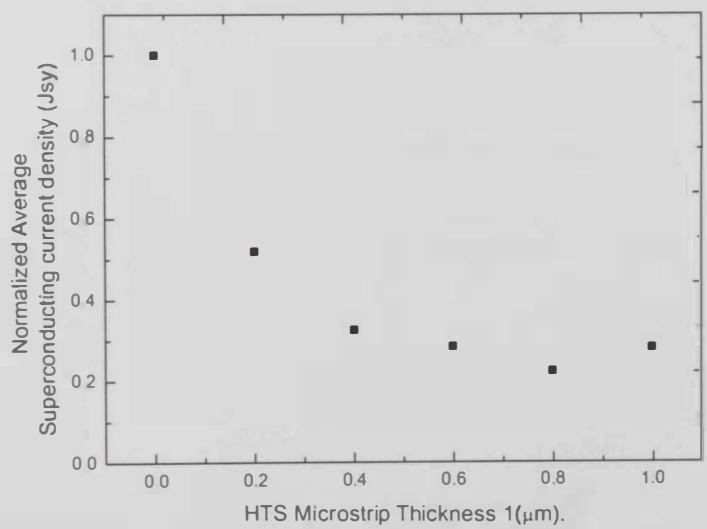

Figure 4.12: Normalized Superconducting current density as function of thickness.

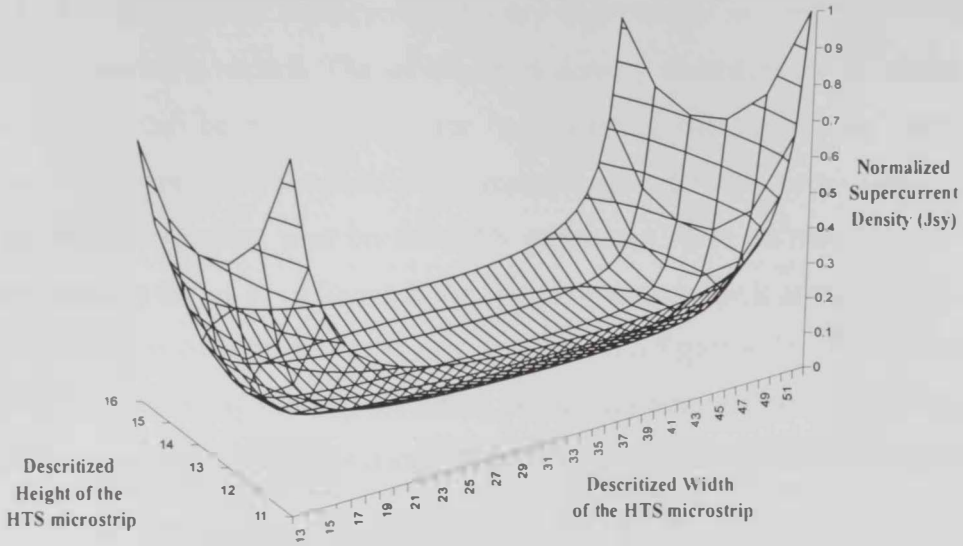

Figure 4.13: Normalized supercurrent density with HTS microstrip width and height.

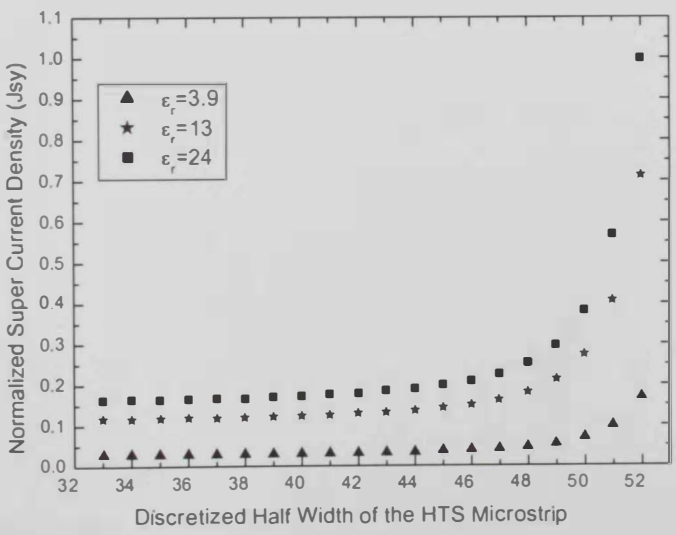

Figure 4.14: Normalized super current density distribution as function of the HTS width at different values of dielectric constant.

4.4.4: Current density as function of temperature:

Temperature variations and its effect on the current density distribution are illustrated in figure 4.15. The normalized supercurrent density distribution as function of width at different temperatures is shown. The supercurrent density decreases as the temperature is increased. This can be explained by the increasing of the penetration depth with temperature. The increase of temperature increases the penetration depth which in turn reduces the superconducting area on the HTS microstrip. The decreasing rate of the supercurrent density seems to be linear at the low temperature but it increased rapidly as we approach the critical temperature as can be seen from figure 4.16. This also can be explained by the increasing of the penetration depth with temperature and that the HTS microstrip loses most of its superconductivity as we approach the critical temperature.

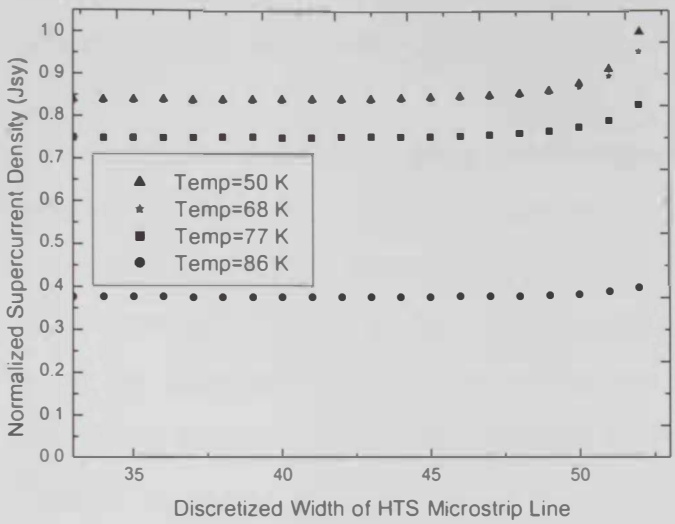

Figure 4.15: Normalized supercurrent density as function of HTS width at different temperatures.

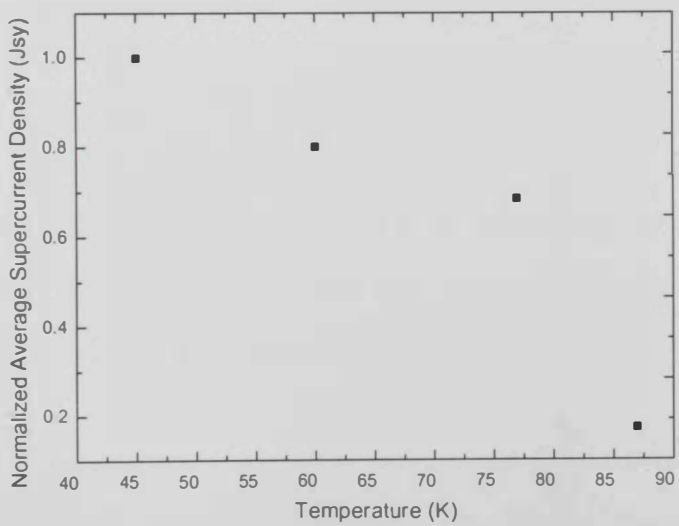

Figure 4.16: Normalized average supercurrent density with temperature.

4.4.5: Surface impedance:

Temperature fluctuation is a critical factor in deciding the reliability of the superconducting microwave devices. Figure 4.17 shows the calculated surface impedance as function of temperature, where it is the quantity of interest for the microwave applications of HTS [12, 40, 45-49].

The concept of surface impedance is used in solving electromagnetic problems when complicated geometries can be reduced to a single boundary with a (usually frequency dependant) boundary impedance value. Problems can be solved using this impedance value without further reference to the geometry beyond the boundary. The impedance value which is required for the solution of this type of problem is the ratio of the tangential electric field E_t and magnetic field H_t at a point on the boundary, and gives the definition of the surface impedance Z_s [12]:

$$Z_s = \frac{E_t}{H_t} \tag{4.16}$$

However, the concept sometimes used when considering surface impedance and connecting it with the penetration depth, which is the case we have, so that the surface impedance can be rewritten as follows:

$$Z_s = \frac{E_t}{\int_0^x J_y(x) * dx} \tag{4.17}$$

Where E_t is the tangential electric field which is E_y in our case, and J_y is the current density in the HTS. Equation 4.17 proves the importance of knowing the current distribution inside the HTS for the calculation of the surface impedance.

In the calculation of the surface impedance, we use the fitting parameters taken from reference [39]. We used equation (3.10) for the calculation of the temperature dependence of the penetration depth $\lambda_L(T)$, and for the calculation of the normal conductivity of the material we used the following relation [30]:

$$\sigma_n(t) = \sigma_n(1)\left\{t^{\gamma-1} + \alpha\left(1 - t^{\gamma}\right)\right\} \quad \text{for } t \le 1 \tag{4.18}$$

where γ is an exponent, α is an empirical parameter, and t is the reduced or normalized temperature ($t=T/Tc$). The fitting parameters used are: (Tc=90K, thickness=0.3 $\mu m\, \sigma_n(1) = 10^6 S/m, \lambda_L(0) = 0.17 \mu m, f = 10 Ghz, \gamma = 2, \alpha = 1$,).

The surface impedance of the HTS microstrip line is very sensitive to temperature fluctuations as can be seen from figure 4.17 especially over the operating temperature 77K up to the critical temperature (*Tc*) of the HTS microstrip line. However, decreasing the operating temperature below 77K would dramatically reduce the sensitivity of the HTS microstrip line to temperature fluctuations. This can be explained by the increase of penetration depth as we increase the temperature. Hence, the magnetic field penetration inside the HTS will increase, which in turn induces oscillations of the electrons which are not bound in Cooper pairs. This oscillation or motion of the unpaired electrons will cause power dissipation which can be characterized by surface resistance.

Our results show a good agreement with the results presented in [39]. However, we used the basic definition of the surface impedance in our model without any approximations. In comparison with the conventional conductors, that has a surface resistance on the order of 20 mΩ at 77K and 10 GHz [12]. The value of the surface resistance of the HTS is much lower, especially for the operating temperature below 77K. This again proves the advantages of using HTS in microwave applications over conventional conductors. Another test was done to verify the accuracy of this model, the fitting parameters used are ($\sigma_n(1) = 4.3X10^6 S/m, \lambda_L(0) = 0.17\mu m, f = 19Ghz, \gamma = 1.5, \alpha = 2.5$, *Tc*=90K and thickness=0.3 μm) [39], the result for the surface resistance is shown in figure 4.18.

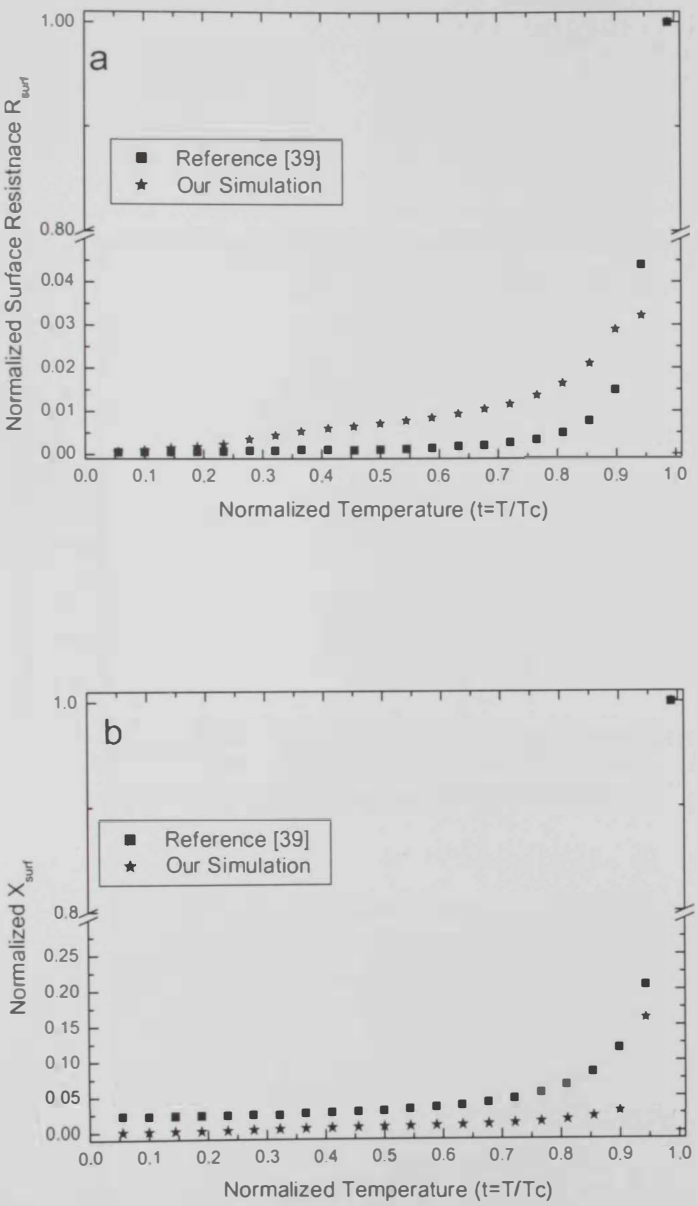

Figure 4.17: Temperature dependence of (a) real part (R_{surf}) and (b) imaginary part (X_{surf}) of the surface impedance. For f=10GHz.

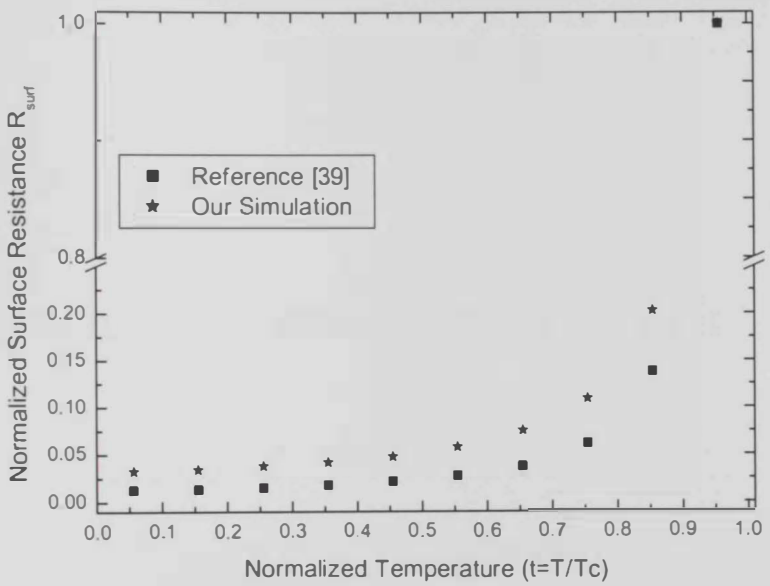

Figure 4.18: Temperature dependence of real part (R_{surf}) of the surface impedance. For f=19 GHz.

Conclusions and Future Work

5.1 Conclusions:

In this thesis, the microwave properties of the HTS microstrip line have been studied numerically using a FDTD code. A theoretical analysis of HTS at high frequencies was discussed, based on the two-fluid model and the London theory in conjunction with Maxwell's equations. The implementation of this model in a FDTD code for a 3-D HTS microstrip line has been presented. The obtained results prove the advantage of using HTS over conventional conductors for the microwave applications.

FDTD method is characterized by its simplicity in concept, ease of implementation and its applicability to the widest range of problems overcoming many other numerical methods. Based on Yee's algorithm and the two time domain Maxwell's curl equations, FDTD has been used in a computer implementation. Because the FDTD method computes the fields throughout the volume and time of interest, any results needed are readily available from the field quantities. Frequency domain parameters are obtained by Fourier transformation of the transient results. This makes FDTD most notable for the analysis of the electromagnetic characteristics of the superconductive microwave devices.

An appropriate physical and mathematical model for HTS has been defined, for suitable integration with the electromagnetic theory. This model takes into consideration the electromagnetic wave propagation and the current distribution inside the HTS. The London Theory and the phenomenological two-fluid model are most notable in this respect, which can predict macroscopically the relation between the local field and the current density.

To have an accurate and robust code, some features need to be considered to accurately model the finite thickness of the HTS microstrip line without any approximation, and to take into consideration the effect of the penetration depth as well. These features include: Time step which depends on the cell size, where a graded mesh generator have been used to discretize the computational space, and the implementation of the absorbing boundary conditions (ABC) to overcome the problem of computer memory limitations and the computational time. A special treatment of the overall stability has been presented.

The HTS properties have been characterized. The longitudinal current density is the maximum component over the other two components. This can be explained by the variation of the magnetic field inside the HTS and the difference in conductivity between the HTS and the substrate. The current density distribution shows a dependence on the thickness of the HTS. It is also affected by the substrate dielectric constant. The relation between temperature variations and current density has been studied as well. The current decreases as the temperature increases, the rate of decay increases rapidly as we approach the critical temperature. This can be explained by the increase of the penetration depth as the temperature is increased.

The advantages of HTS over ordinary conductors have been proven throughout the results obtained; where the attenuation constant and the surface resistance of the HTS are at least one order of magnitude lower than those of ordinary conductors at the same operating temperature and frequency.

5.2 Recommendations and Future Work:

The unavailability of an accepted accomplished theory for the High-Tc superconductivity reveals that a comprehensive and accurate study that sets all the standards for the design of HTS microwave devices is needed. This study could include the following areas:

1. Accepted theory for the High-Tc superconductivity. The well known two-fluid model, the London theory and the Ginzburg–Landau (GL) theory are still phenomenological, that is quantitatively adequate to the macroscopic properties but not using its microscopic nature.
2. On the technological side, it is well known that the HTS films are deposited on an appropriate substrate. In addition of having good microwave properties, the substrate should be compatible with good film growth. The film itself should be uniform with almost free defects and twining as possible.
3. The study could be extended to take into consideration the effect of the anisotropy in the HTS microstrip line and in the substrate as well.
4. The study could be extended also to include the nonlinearities in HTS.
5. One important step is to use the developed code in designing HTS microwave devices such as resonators and filters.

6. A more general study could take into consideration the defects and the surface barriers appearing which affect greatly the current distribution.
7. Experiments could be done to fabricate the HTS microstrip line and then carry out some measurements of the parameters modeled.

References:

[1] Bardeen J., Cooper L. N. and Schrieffer J. R. ' Theory of superconductivity', Phys. Rev., 108, 1175-1204, 1957.

[2] Peter Schm¨user, Institut f¨ur Experimentalphysik, Universit¨at Hamburg, 'Basic Principles of RF Superconductivity and Superconducting Cavities'

[3] Z. Y. Shen, *High Temperature Superconducting Microwave Circuits.* Norwood, MA: Artech House, 1994.

[4] Mohan V. Jacob, Janina Mazierska, Nick Savvides, Shigetoshi Ohshima and Shinichro Oikawa, 'Comparison of microwave properties of YBCO films on MgO and LaAlO3 Substrates', physica C.

[5] T. P. Orlando and K. A. Delin, *Foundations of Applied Superconductivity.* Reading, MA: Addison-Wesley, 1991.

[6] T. Van Duzer and C. W. Turner, 'Principles of Superconductive Devices and Circuits'. Englewood Cliffs, NJ: Prentice-Hall, 1999.

[7] Mohamed A. Megahed, and Samir M. El-ghazaly, ' nonlinear analysis of microwave superconductor devices using full-wave electromagnetic model', IEEE Trans. Microwave theory Tech., vol. 43, NO. 11, pp.2590-2599, November 1995.

[8] Samir M. El-Ghazaly, Robert B. Hammond and Tatsuo Itoh, ' analysis of superconducting microwave structures: application to microstrip lines', IEEE Trans. Microwave theory Tech., vol. 40. NO. 3, pp. 499-508, march. 1992.

[9] Shau-Gang Mao, Jeng-Yi Ke, and Chun hsiung Chen, ' propagation characteristics of superconducting microstrip lines', IEEE Trans. Microwave theory Tech., vol. 44. NO. 1, pp.33-40, January 1996.

[10] David R. chase, ' HTS: on line and operational', RFdesign.com

[11] Yoshiki UENO, Kenshi SAITO, Nobuyoshi SAKAKIBAR, Mitsunari OKAZAKI, and Masayuki AOKI, 'HTS Microstrip line filter for mobile telecommunication', IEICE TRANS ELECTRON., VOL. E81-c, No. 10 OCTOBER 1998.

[12] M.J. Lancaster, ' passive microwave device of HTS', (Camb. uni. press, 1997)

[13] J. Kessler, R. Dill and P. russer, ' field theory investigation of hight-Tc, superconducting coplanar waveguide transmission lines and resontors', IEEE Trans. Microwave theory Tech., vol. 39. pp.1566-1574, Sept. 1991

[14] L. H. Lee, S. M. Ali, W. G. lyons, ' full wave characterization of high-Tc superconducting transmission lines', IEEE. Trans. Appl. Superconductivity, vol. 2, pp. 49-57, june 1992.

[15] L. H. Lee, S. M. Ali, W. G. lyons, D. E. Oates, and J. D. Goettee, ' Analysis of superconducting transmission line structures for passive microwave device applications', IEEE. Trans. Appl. Superconductivity, vol. 3. pp. 2782-2787, Mar. 1993.

[16] Laurence H. Lee, W. Gregory Lyons, Terry P. Orlando, Sami M. Ali, and Richard S. Withers. ' Full-wave analysis of superconducting microstrip line on anisotropic substrate using equivalent surface impedance approach', IEEE Trans. Microwave theory Tech., vol. 41. NO. 12, pp.2359-2367, Dece. 1993

[17] J. M. Pond, C. M. krowne, and W. L. Cater, ' On the application of complex resistive boundary conditions to model transmission lines consisting of very thin superconductors', IEEE Trans. Microwave theory Tech., vol. 37. NO. 1, pp. 181-190, Jan. 1989.

[18] Z. Cai and J. Bornemann, ' Generalized spectral-domain analysis for multilayered complex media and high-Tc superconductor applications', IEEE Trans. Microwave theory Tech., vol. 40. NO. 12, pp.2251-2257, Dece. 1992.

[19] N. Enomoto , N. Amemiya, ' Electromagnetic field analysis of rectangular high Tc superconductor with large aspect ratio', Physica C 412–414 (2004) 1050–1055.

[20] Shujun Xiao and Ruediger Valdieck,' 3D FDTD Simulation of superconductors coplanar waveduides', 1995 IEEE MTT-Digest.

[21] Mohamed A. Megahed, and Samir M. El-ghazaly, ' analysis of anisotropic HTS palanar structure on sapphire anisotropic substrates', IEEE Trans. Microwave theory Tech., vol. 43, NO. 8, pp.1989-1992, august 1995.

[22] Y.Okazaki, K.Suzuki, and Y.Enomoto, ' Superconducting Microstrip Resonator Investigated By FDTD Electromagnetic Field Simulator', IEEE Trans. On Applied Superconductivity, vol.9, No.2, pp.3034-3037, June 1999.

[23] K. S. Yee 'numerical solution of initial boundary value problems involving Maxwell's equations in isotropic media'. IEEE Trans. Antenna prop., vol. AP-14, no. 3, pp. 302-307, may 1966.

[24] Mousa Issa M. Hussein. 'Time-domain based finite differencing technique and its application to electromagnetic problems'. Phd thesis. University of Manitoba, Canada 1995.

[25] Jiayuan fang. 'Time domain finite difference computation for Maxwell's equations'. PhD thesis, university of California at Berkeley.

[26] Karl S. kunz, Raymond J. Luebbers, 'Finite difference time domain method for electromagnetics'. 1993 By CRC Press, Inc.

[27] A. Taflove and M. E. Brodwin, 'Numerical Solution of Steady-State Electromagnetic Scattering Problems using the Time-Dependent Maxwell's Equations', IEEE Transactions on Microwave Theory and Techniques, MTT-23, 8, 1975, pp. 623-630.

[28] G. Mur. 'Absorbing boundary conditions for the finite difference approximation of the time domain electromagnetic field equations'. IEEE Trans Electromag. Compat. Vol. 23, pp. 377-382, 1981.

[29] Kenneth K. Mei and J. Fang. 'Super-absorption a method to improve absorbing boundary conditions'. IEEE Trans. Antenna propagate., vol. 40, pp. 1001-1010, 1992.

[30] J. P. Berenger. 'A perfectly matched layer for the absorbing of electromagnetic waves'. J. computational phys., 1994.

[31] D. S. Katz, E. T. Thiele, and A. Teflove. 'Validation and extension to three dimensions of the berenger PML absorbing boundary condition for FD-TD meshes'. IEEE Micr. Guid. Lett., vol. 4, pp. 268-270, 1994.

[32] London F. and London H. physica, 2, 341, 1935.

[33] London F. and London H. Proc. Roy. Soc. (lond), A149, 71, 1935

[34] London H. production of heat in superconductors by alternating currents, Nature, 133, 497, 1934.

[35] Pippard A. B.' the surface impedance of superconductors and normal metals at high frequencies. Parts I, II and III. Proc. Roy. Soc., A191 370-415, 1947.

[36] Mattis D. C. and bardeen J. ' Theory of the anomalous skin effect in normal and superconducting metals', Phys. Rev. 111, 412-417, 1958.

[37] Bednoz J. G. and muller K. A. 'Possible High Tc superconductivity in the Ba-La-Cu-O system', Phys., B64, 189, 1986.

[38] Michael Tinkham, 'introduction to superconductivity'. 2nd edition.

[39] Orest G. Vendik, Irnia B. vendik, and Dimitri I. Kaparkov, 'Emperical model of the microwave properties of HTS', IEEE Trans. Microwave theory Tech., vol. 46. NO. 5, pp. 469-478, may 1998.

[40] J. M. Pond, K. R. Carrol, J. S. Horwitz, D. B. Chirsey, M. S. Osofsky, and V. S. Cestone, "Penetration depth and microwave loss measurement with a YBCO/LaAlO/ YBCuO trilayer transmission line," Appl. Phys. Lett., vol. 59, pp. 3033–3036, Dec. 2, 1991.

[41] J. Y. Lee and T. R. Lemberger, "Penetration depth λ(T) of YBCO films determined from the kinetic inductance," Appl.
Phys. Lett., vol. 62, pp. 2419–2421, May 10, 1993.

[42] T. Kisu, T. Iinuma, K. Enpuku, K. Yoshida, and K. Yamafumi, "Magnetic penetration depth and critical current in YBCO thin films," IEEE Trans. Appl. Superconduct., vol. 3, pp. 2961–2964, Mar. 1993.

[43] S. D. Brorson, R. Buhleier, J. O. White, L. E. Trofimov, H.-U. Habermeire, and J. Kuhl, "Kinetic inductance and penetration depth of thin superconducting films measured by THz-pulse spectroscopy," Phys. Rev. B, Condens. Matter vol. 49, pp. 6185–6187, Mar. 1993.

[44] S. El-Ghazaly, T. Itoh, and R. Hammond, ' design considerations for high Tc superconductor microstrip lines based on current distribution'. Microwave and optical tech. lett. July 1991.

[45] O.G. Vendik, I.B. Vendik and D.V. Kholodniak, 'applications of high-temperature superconductors in microwave integrated circuits', Mater.Phys.Mech.2 (2000) 15-24.

[46] L. Lee S. Ali and W. Lyons, ' full-wave characterization of high-Tc superconducting transmission lines'. IEEE Trans. Appl. Superconduct., vol. 2, no. 9, pp. 49-57, 1992.

[47] I. Vendik, 'phenomenological model of the microwave surface impedance of HTS thin films', supercond. Sci. Tschnol. 13 (200) 947-982.

[48] Jian-Guo ma and Ingo Wolff, 'modeling the microwave properties of superconductors', IEEE Tran. On microwave theory and techniques, vol. 43, no. 5, may 1995.

[49] J. I. Gittleman, J. R. Matey, 'modeling the microwave properties of the YBCO superconductors' J. Appl. Phys. 65 (2), 15 January 1989.

التوصيف والنمذجة المايكرويفية
لشرائط الموصلات الفائقة الرقيقة ذات درجة الحرارة العالية

الخلاصة

بسبب درجة الحرارة الحرجة العالية التي تستطيع الموصلات الفائقة ان تصل لها، فان تطبيقاتها التكنولوجية قد اتسعت. وأحد أهم هذة التطبيقات يتمثل في استخدامها بشكل شرائط رقيقة لصناعة الاجهزة التي تستخدم في تطبيقات الموجة الدقيقة (Microwave). وتتركز أهميتها من خلال الفقدان القليل للطاقة خلال انتقال الاشارة داخل هذة الشرائط. فعلى سبيل المثال فان المقاومة السطحية لهذة الموصلات الفائقة اقل كثيرا من المقاومة السطحية للموصلات العادية. ومن هنا يأتي الاهتمام الزائد في تطبيقاتها وخاصة في مجال الاجهزة الالكترونية.

ان توصيف ونمذجة سلوك هذة الموصلات الفائقة لا يزال مجال بحث حتى الان. وذلك بسبب النقص في معرفة آلية التوصيل الكهربائي. فعلى سبيل المثال فان فقدان الطاقة، فيما يعرف بالموصلات الفائقة من النوع الثاني، يحصل نتيجة حركة التيار (التي تكون على شكل البراكين) الناتج عن مجال مغناطيسي خارجي. ومن هنا تبرز أهمية معرفة آلية التوصيل لا بل والتوزيع الصحيح لكثافة التيار في هذة الموصلات الفائقة. وبسبب عدم وجود مفهوم فيزياني لطبيعة التفاعل والتزواج بين الالكترونات داخل هذة الموصلات الفائقة ذات درجة الحرارة العالية، فان العوامل المختلفة الاخرى كالموصلية الكهربائية ودرجة الاختراق للمجال المغناطيسي داخل هذة الموصلات الفائقة يجب أن تؤخذ بعين الاعتبار.

في هذة الرسالة، سيتم دراسة فقدان الطاقة خلال انتقال الاشارة داخل هذة الموصلات الفائقة ذات درجة الحرارة الحرجة العالية من خلال احد طرق النمذجة الحسابية المعروفة. وهذة الطريقة تعرف باسم " Finite Difference Time Domain Method"". مع الاخذ بعين الاعتبار العوامل المختلفة الاخرى مثل: المقاومة السطحية وتوزيع كثافة التيار على عرض وارتفاع هذة الشرائط. وتأثير درجة الحرارة عليهما.

جامعة الإمارات العربية المتحدة

عمادة الدراسات العليا

برنامج ماجستير علوم المواد

التوصيف والنمذجة المايكرويفية
لشرائط الموصلات الفائقة الرقيقة ذات درجة الحرارة العالية

رسالة مقدمة من الطالب:

ثامر موسى بدارنه

الى جامعة الإمارات العربية المتحدة

استكمالا لمتطلبات الحصول على درجة الماجستير في علوم وهندسة المواد

2005-2006